Published in final edited form as:
Nature. 2019 June 28; 570(7760): 246–251. doi:10.1038/s41586-019-1263-7.

Distinct fibroblast subsets drive inflammation and damage in arthritis

Adam P Croft[1], **Joana Campos**[1], **Kathrin Jansen**[2], **Jason D Turner**[1], **Jennifer Marshall**[1], **Moustafa Attar**[2], **Loriane Savary**[1], **Corinna Wehmeyer**[1], **Amy J. Naylor**[1], **Samuel Kemble**[1], **Jenefa Begum**[1], **Kerstin Duerholz**[1], **Harris Perlman**[3], **Francesca Barone**[1], **Helen M McGettrick**[1], **Douglas T Fearon**[4], **Kevin Wei**[5], **Soumya Raychaudhuri**[5], **Ilya Korsunsky**[5], **Michael B Brenner**[5], **Mark Coles**[2], **Stephen N Sansom**[2], **Andrew Filer**[1,6], **Christopher D Buckley**[1,2]

[1]Rheumatology Research Group, Institute for Inflammation and Ageing, College of Medical and Dental Sciences, University of Birmingham, Queen Elizabeth Hospital, Birmingham, B15 2WD, UK

[2]The Kennedy Institute of Rheumatology, University of Oxford, Oxford. UK

[3]Department of Medicine, Division of Rheumatology, Northwestern University, Feinberg School of Medicine Chicago, IL, USA

[4]Cold Spring Harbor Laboratory, 1 Bungtown Road, Cold Spring Harbor, NY 11724 USA

[5]Division of Rheumatology, Immunology, and Allergy, Brigham and Women's Hospital, Harvard Medical School, Boston, MA 02115, USA

Correspondence and requests for materials should be addressed to CDB (c.d.buckley@bham.ac.uk).

Data availability

STIA single cell and bulk fibroblast RNA sequence data that support the findings of this study have been deposited in Gene Expression Omnibus (GEO) with the accession codes GSE129087 and GSE129451. Source data for figure(s) 1,2,4 and extended data 1,2,3 and 10 are provided with the paper.

Code availability

The source code repository of the computational pipeline for single cell data analysis and integration is located at https://www.github.com/sansomlab/tenx/.

Author Contributions

APC conceived the project, performed experiments, analysed data, and wrote the manuscript. JC performed experiments, analysed data, and helped write the manuscript. KJ analysed the single cell RNA sequencing data and helped to write the manuscript. JDT performed flow cytometry on human synovial biopsy tissue. JM performed immunofluorescence microscopy. MA performed single cell capture and library preparation. LS performed tissue histology and microscopy. CW and AJN performed osteoclast differentiation assays. SK assisted with the CIA experimental arthritis model. JB performed micro CT analysis. KD performed flow cytometry from CIA mouse joints. HP generated serum from KBxN mice. FB and HMM helped in the design and interpretation of experimental mouse data. DTF generated FAPα-DTR mouse. KW performed and analysed mass cytometry of human synovial biopsy tissue. SR and IK helped generate, analyse and interpret human single cell transcriptomic data. MB and MC provided critical interpretation of experimental data. SNS supervised the design, execution, analysis and interpretation of the single-cell transcriptomics experiments and helped write the manuscript. AF participated in study design, patient recruitment, sample acquisition, and review of the data. CDB conceived the project, supervised the work, analysed data, and co-wrote the manuscript. All authors discussed the results and commented on the manuscript

Author information

Reprints and permissions information is available at www.nature.com/reprints.

The authors have no competing financial interests.

Europe PMC Funders Author Manuscripts

[6]University Hospitals Birmingham NHS Foundation Trust, Birmingham B15 2GW, UK

Summary

The identification of lymphocyte subsets with non-overlapping effector functions has been pivotal to the development of targeted therapies in immune mediated inflammatory diseases (IMIDs)[1,2]. However it remains unclear whether fibroblast subclasses with non-overlapping functions also exist and are responsible for the wide variety of tissue driven processes observed in IMIDs such as inflammation and damage[3–5]. Here we identify and describe the biology of distinct subsets of fibroblasts responsible for mediating either inflammation or tissue damage in arthritis. We show that deletion of FAPα$^+$ fibroblasts suppressed both inflammation and bone erosions in murine models of resolving and persistent arthritis. Single cell transcriptional analysis identified two distinct fibroblast subsets within the FAPα$^+$ population: FAPα$^+$ THY1$^+$ immune effector fibroblasts located in the synovial sub-lining, and FAPα$^+$ THY1$^-$ destructive fibroblasts restricted to the synovial lining layer. When adoptively transferred into the joint, FAPα$^+$ THY1$^-$ fibroblasts selectively mediate bone and cartilage damage with little effect on inflammation, whereas transfer of FAPα$^+$ THY1$^+$ fibroblasts resulted in a more severe and persistent inflammatory arthritis, with minimal effect on bone and cartilage. Our findings describing anatomically discrete, functionally distinct fibroblast subsets with non-overlapping functions have important implications for cell based therapies aimed at modulating inflammation and tissue damage.

Keywords

Synovial fibroblasts; inflammation; arthritis; transcriptomics; rheumatoid arthritis

Non-hematopoietic, tissue resident fibroblasts, contribute to the pathogenesis of many diseases and are known to develop epigenetically imprinted, site and disease specific phenotypes[6–8]. Rheumatoid arthritis (RA) is a prototypic IMID[6] in which synovial fibroblasts (SFs) contribute to both joint damage[7,8] and inflammation[9]. We found that expression of fibroblast activation protein α (FAPα), a cell membrane dipeptidyl peptidase[10], was significantly higher in both synovial tissue and cultured SFs isolated from patients who fulfilled classification criteria for RA, compared to patients in whom joint inflammation resolved (Fig 1a,b,c), suggesting that FAPα expression may associate with a pathogenic fibroblast phenotype.

To map the expression of FAPα expressing cells in the RA synovium we used mass cytometry (CyTOF), together with a combination of podoplanin (PDPN) and THY1 (CD90) to discriminate sub-lining layer (SL, THY1$^+$) from lining layer (LL, THY1$^-$) fibroblasts, as in previous studies[4,5,11]. FAPα co-localized with PDPN in both the LL and SL cells (Fig 1d). A small subset of pericytes (defined as CD45$^-$ PDPN$^-$ and THY1$^+$) also expressed FAPα. These findings were confirmed by confocal analysis in RA synovial tissue (Fig 1e).

To determine the role of FAPα$^+$ SFs in arthritis, we used serum transfer induced arthritis (STIA)[12] in a transgenic FAPα luciferase-DTR reporter mouse[13]. FAPα expression (bioluminescence) increased during the course of arthritis (Fig 1f,g) and correlated with the severity of ankle joint swelling (Fig 1h). Synovial expression of FAPα was either low or

Europe PMC Funders Author Manuscripts

undetectable under resting conditions (extended data 1a) but increased in SM and focal areas of pannus tissue invading cartilage and bone during inflammation (Fig 1i,j and extended data 1a). FAPα expression was restricted to mesenchymal cells ($CD45^-$) (extended data 1b-f) and the number of $FAP\alpha^+$ fibroblasts increased during inflammation returning to baseline levels with resolution of inflammation (Fig 1k and extended data 1c,d), confirming that FAPα is a biomarker of tissue inflammation (Fig 1f-k, extended data 1a,c,d).

In the murine synovium, THY1 expression also distinguished SL from LL fibroblasts, with FAPα expressed in both cellular compartments (extended data 1e,f,g). *Pdpn*, *Fap* and *Thy1* mRNA showed a significantly higher induction in the inflamed SM (Fig 1l) and expression positively correlated with joint swelling (Fig 1m). A significant increase in the proliferation of both $THY1^-$ $FAP\alpha^+$ (LL) and $THY1^+$ $FAP\alpha^+$ (SL) cells was observed during inflammation, with very little change in the number of FAPα expressing pericytes (Fig 1n). The severity of joint inflammation positively correlated with the total number of $FAP\alpha^+$ $THY1^+$ expressing cells but not $FAP\alpha^+$ $THY1^-$ cells (extended data 1h). The extent of cartilage damage did however correlate with the number of $FAP\alpha^+$ $THY1^-$ cells (extended data 1i), whereas the severity of bone erosion positively correlated with the number of $FAP\alpha^+$ $THY1^+$ cells and not $FAP\alpha^+$ $THY1^-$ cells (extended data 1j). Collectively these data suggest the expansion of a potentially pathogenic population of SFs is marked by expression of PDPN, FAPα and THY1.

To determine the functional role of $FAP\alpha^+$ fibroblasts *in vivo* we selectively deleted $FAP\alpha^+$ cells during arthritis (extended data 1k-m). Deletion led to a significant reduction in the cellularity of the SM (extended data 1n-p), attenuated synovial inflammation and accelerated resolution in both the resolving (Fig 2a) and persistent models of STIA (Fig 2b), with the same effect observed regardless of the stage of arthritis at time of deletion (extended data 2a,b). However, deletion prior to induction of arthritis, had no effect on joint thickness (extended data 2c), an observation consistent with the low numbers of $FAP\alpha^+$ cells in the SM under resting conditions (extended data 1a,c). Deletion of $FAP\alpha^+$ cells reduced structural joint damage (cartilage and bone damage), inflammatory bone re-modelling, pannus formation (Fig 2c,d and extended data 2d-f), osteoclast numbers (Fig 2d, extended data 2g,h), and reduced expression of osteoclast and osteoblast bone markers in whole joint tissue (extended data 2i).

$FAP\alpha^+$ cell deletion led to reduced leucocyte infiltration (Fig 2e), negatively correlated with the severity of joint inflammation (Fig 2f) and was associated with a reduction in the number of both LL and SL fibroblasts, with no significant change in pericyte numbers (Fig 2g). Circulating blood monocyte number and phenotype were unchanged (extended data 3a), excluding any potential indirect effects of myelosuppression. Accompanying these changes was a marked reduction in the number of synovial leucocytes, specifically neutrophils, macrophages, $CD11b^+$ dendritic cells and monocytes, but not eosinophils (extended data 3b for gating strategy, Fig 2h for resolving STIA model data and extended data 3c, for persistent model), as well as a reduction in the percentage of MHC Class II expressing macrophages (persistent model: extended data 3c and resolving model: extended data 3e). There were very few remaining macrophages in the SM following $FAP\alpha^+$ cell deletion (extended data 3d) and those remaining had a more anti-inflammatory phenotype (extended

data 3f). These cellular changes in the synovium were accompanied by a marked reduction in pro-inflammatory chemokines, cytokines, RANKL and MMPs (Fig 2i), demonstrating that synovial FAPα$^+$ cells are a significant source of these proteins.

To exclude an indirect effect of systemic deletion of FAPα$^+$ cells, we delivered DTx locally to the joint. This resulted in cell deletion in the SM but not in draining or distant lymph nodes (extended data 3g) and did not result in systemic cachexia (extended data 3h), reported previously after systemic FAPα$^+$ cell deletion[13]. Local deletion had the same effect on joint inflammation and bone damage with no effect observed in non-injected joints or following administration of DTx in non-arthritic mice (extended data 3i-k).

We next explored whether both THY1$^-$ FAPα$^+$ (LL) and THY1$^+$ FAPα$^+$ (SL) fibroblast populations contribute equally to inflammation and bone damage. We first performed single cell RNA sequencing of CD45$^-$ non-haematopoietic cells from inflamed mouse synovium. After assigning identities to all cell clusters (Fig 3a, extended data 4a-d, 5, 6, supplementary table 1), targeted re-analysis of the fibroblast populations, based on expression of known fibroblast markers, revealed the existence of five distinct subgroups (Fig 3b, extended data 6 and 7a-d, supplementary table 1). Gene ontology (GO) analysis of significant cluster marker genes suggested a diversification of function between the subsets. F1 fibroblast marker genes were over-represented in categories related to bone, cartilage and extra-cellular matrix formation. F2 cells were strongly characterised by expression of inflammatory genes including those involved in “cytokine production” and “regulation of leukocyte chemotaxis”. Meanwhile, F3 fibroblasts showed an enrichment for genes involved in the “complement activation” and “vasculogenesis” biological processes. F4 fibroblasts expressed genes characteristic of an actively cell cycling population. Finally, F5 fibroblasts displayed a phenotype that included a distinctive over-representation of genes associated with “acid secretion” and “hydrogen transport” (Fig 3c, supplementary table 2).

Examination of the top cluster marker genes allowed us to easily differentiate these five subsets at the mRNA expression level (Fig 3d). While *Pdpn* and *Fap* were expressed by all of the fibroblast subsets, *Thy1* was expressed selectively by F1-F4 fibroblasts but not F5 fibroblasts (Fig 3d, extended data 6), suggesting that we could use THY1 as a marker to discriminate the LL F5 subset from the four SL clusters (F1-F4). We also examined the expression of other known fibroblast markers across the subsets as well as the specific expression of selected chemokines (extended data 7a,c).

We next examined the potential development relationship between the different fibroblast subsets using a diffusion map (Fig 3e). Application of the pseudotime algorithm Slingshot[14], identified two single-branch trajectories comprising of F1-F2-F3-F4 and F1-F2-F5. Existence of the F1-F2-F5 trajectory is consistent with the diffusion map topology and analysis of genes differentially expressed along this trajectory (extended data 8a) showed that cells of cluster F2 have overlapping profiles with those of F1 and F5.

To investigate the existence of homologous fibroblast subsets in human arthritis, we selectively re-analysed data from RA patient synovial biopsies[15]. This analysis identified five distinct sub-populations (extended data 8b-e). Correlation of orthologous (one-to-one)

cluster markers from the human and mouse datasets identified three homologous populations of fibroblasts (Fig 3f) that share distinctive gene expression profiles (Fig 3g). The homologous clusters comprised of (i) LL fibroblasts (Mm STIA F5 – Hs RA F4), (ii) *Cd34*+ve SL fibroblasts (Mm STIA F3 – Hs RA F5) and (iii) *Col11a1*+ve SL fibroblasts (Mm STIA F1 – Hs RA F2).

To confirm the validity of using PDPN, THY1 and FAPα as a cassette of cell surface markers to discriminate LL and SL fibroblasts, we performed ultra-low input RNA sequencing on purified PDPN^{+}, FAPα$^{+/-}$ and THY1$^{+/-}$ cell populations (extended data 9a-d, supplementary tables 3-6). Principal component analysis of transcriptional differences confirmed that the subsets defined by expression of THY1 represented transcriptionally distinct populations with the most obvious separation between THY1^{+} versus THY1^{-} populations regardless of FAPα expression (extended data 9b). The THY1^{+} cell population showed expression of many chemokines and cytokines and expressed F1-F4 subset specific genes (extended data 9c,d). In contrast, THY1^{-} cell gene expression was consistent with F5 fibroblasts associated genes such as *Prg4*, *Clic5* and *Tspan15* as well as genes associated with cartilage and bone erosion. Therefore the greatest determinant of the transcriptional profile of SFs appeared to be their anatomical location in the SM (as defined by THY1 expression).

As predicted from the single cell transcriptome analysis, FAPα^{+} THY1^{+} subsets had an immune effector profile with higher expression of chemokines as well as cytokines including: *Il6*, *Lif*, *Il33* and *Il34*. In contrast, FAPα^{+} THY1^{-} expressing subsets expressed higher levels of *Ccl9* and *TNFSF11* both potent inducers of osteoclast activity, as well as *Mmp3*, *Mmp9* and *Mmp13*; matrix metalloproteinases involved in cartilage degradation (extended data 9d). These findings were validated, where possible for protein expression (Fig 4a). FAPα^{+} THY1^{-} cells also expressed RANKL on their surface, secreted higher levels of RANKL, exhibited a significantly increased RANKL/OPG ratio (Fig 4b,c) and stimulated osteoclast differentiation/activation *in vitro*, leading to significantly more resorption of hydroxyapatite matrix *in vitro* (Fig 4d). Taken together these results support the concept that THY1^{-} and THY1^{+} cells might perform distinct non-overlapping functions *in vivo.*

To directly test this hypothesis we injected PDPN^{+} FAPα^{+} THY1^{-} or PDPN^{+} FAPα^{+} THY1^{+} cells into the inflamed ankle joint of mice during STIA. Injection of PDPN^{+} FAPα^{+} THY1^{+} cells resulted in more severe and sustained joint swelling (Fig 4e), with higher levels of leucocyte infiltration (Fig 4f) but with little effect on bone and cartilage destruction (Fig 4g,h). In contrast, the injection of PDPN^{+} FAPα^{+} THY1^{-} cells had no effect on the severity or temporal dynamics of joint inflammation (Fig 4e,f), but did result in increased osteoclast activity and increased structural joint damage (Fig 4g,h). The same effects were observed following the injection of each cell population into an inflamed ankle joint of mice with collagen induced arthritis (CIA) (extended data 10a,b). In this case, injection of PDPN^{+} FAPα^{+} THY1^{+} also resulted in increased effector CD4^{+} T cells, reduced Foxp3^{+} Tregs, and a global increase in neutrophil and macrophage cell infiltration (extended data 10c).

Following joint injection, cells engrafted into the SM, remaining largely at the site of injection and were detectable up to 14 days after injection (extended data 10d). They

maintained their original cell phenotype with regards to THY1 expression (extended data 10e) but did not preferentially localise to any specific anatomical compartment of the SM. No significant difference in the level of engraftment or viability between injected cell populations was observed (extended data 10f). Collectively, these data suggest that in pathological conditions PDPN^{+} FAPα^{+} THY1^{+} expressing cells assume an immune effector role capable of sustaining inflammation through the production of a distinct repertoire of chemokines and cytokines, whereas PDPN^{+} FAPα^{+} THY1^{-} cells are bone effector cells that mediate joint damage.

In support of this conclusion, and as validation of the relevance of our findings to human disease, we identified an expanded population of PDPN^{+} FAPα^{+} THY1^{+} immune effector fibroblasts in the synovia of patients with RA, in whom joints are persistently inflamed, compared to patients with osteoarthritis (OA), a disease characterised predominately by cartilage damage rather than inflammation (Fig 4i). The expansion of PDPN^{+} THY1^{+} FAPα^{+} cells positively correlated with markers of systemic and tissue inflammation (Fig 4j).

In summary, we have identified and described the pathological significance of fibroblast heterogeneity in RA, an IMID in which inflammation and damage play key pathogenic roles. We describe discrete, anatomically distinct subsets of fibroblasts with non-overlapping effector cell functions including joint and cartilage damage (production of MMPs and induction of osteoclastogenesis) and immuno-inflammatory regulation (production of inflammatory cytokines and chemokines). These findings provide the unpinning justification for the development of therapies that selectively target deletion or replacement of different mesenchymal subpopulations in a wide range of diseases.

Methods

Human subjects research

Human subjects research was performed according to the Institutional Review Boards at Partners HealthCare, Hospital for Special Surgery and the West Midlands and Black Country Research Ethics Committee via approved protocols with appropriate informed consent. The study was compliant with all relevant ethical regulations. Synovial tissues and clinical outcome data of patients included in the early arthritis patient cohort in Birmingham (BEACON) were used in this study[10]. All patients were naïve to treatment with disease modifying anti-rheumatic drugs (DMARDs) and corticosteroids at inclusion. Control synovial tissue was obtained from uninflamed joints of patients with joint pain but normal imaging studies undergoing exploratory arthroscopy. Samples from patients with osteoarthritis were obtained from arthroplasty procedures and tissue from patients with RA obtained by ultrasound guided synovial biopsy as previously described[10,15].

Human synovial tissue processing, histological analysis and immunofluorescence staining

Synovial tissue samples were frozen in Tissue-Tek OCT medium (Miles, Elkhart, IN) or formalin fixed and paraffin embedded (FFPE).

For immunohistochemistry, antigen retrieval was performed at pH 9 on FFPE sections using Tris-EDTA, 0.05% Tween 20 (10mM Tris Base, 1mM EDTA Solution, 0.05% Tween 20). Sections were stained using anti-FAPα (R&D) and anti-goat Horseradish peroxidase (HRP) (Dako). HRP staining was developed using the ImmPACT DAB Peroxidase HRP Substrate (Vector Labs). Images were acquired using the Zeiss Axio Scan and analysed with Zen lite 2012 software (Zeiss). Number of pixels was quantified and divided by a manually defined tissue area and the average number of pixels per unit area (pixel/UA) was calculated.

For immunofluorescence, acetone fixed frozen sections were incubated with anti-FAPα (F11-24, eBioscience), anti-PDPN (NZ-1.3, eBioscience) and anti-THY1 (Thy-1A1, R&D). These were detected with goat anti-mouse IgG1 FITC, anti-mouse IgG2a TRITC and anti-mouse IgG2b Cy5 (all Southern Biotech). To increase signal from FITC-channel, goat anti-FITC Alexa-488 antibody (Invitrogen) was used. Images were acquired using a Zeiss LSM 510 confocal microscope and ZEN pro 2011 imaging software.

Human fibroblast cell culture

Human fibroblasts were isolated as described[18] and cultured in Dulbecco's modified Eagle's medium (DMEM) (Sigma-Aldrich) with 2% fetal bovine serum (FBS; Gemini), 2 mM L-glutamine, antibiotics (penicillin and streptomycin), and essential and non-essential amino acids (Life Technologies). Fibroblast lines at passage 3 or 4 were used for *in vitro* experiments.

Enzymatic digestion of human synovial tissue

Synovial tissue samples were disaggregated into single cell suspension as previously described[19]. Synovial tissue fragments were separated using Liberase TL (100μg/mL; Sigma-Aldrich) and DNase I (100μg/ml; Roche) in RPMI in a 37°C water bath for 30min. Single cell suspensions were assessed for cell quantity and cell viability.

Mass cytometry on human synovial cells

Cryopreserved disaggregated human synovial cells were thawed into RPMI + 10% FBS (HyClone). Viability was assessed and cells were stained with primary antibody cocktails at 1:100 dilution (CD45, metal 89Y, clone HI30; PDPN, metal 156Gd, clone NC-08; FAP, metal 147Sm, Poly; THY1, metal 162Dy, clone 5E 10). All antibodies were obtained from the Longwood Medical Area CyTOF Antibody Resource Core. Cells were fixed and permeabilized using the eBioscience Transcription Factor Fix/Perm Buffer followed by staining for intracellular markers. Cells were re-fixed in formalin (Sigma-Aldrich), washed with Milli-Q water, and analyzed on a Helios (Fluidigm). Mass cytometry data were normalized using EQ™ Four Element Calibration Beads (Fluidigm) viSNE analyses were performed on cytometry data, using the Barnes-Hut SNE implementation on Cytobank (www.cytobank.org). All biaxial gating was performed using FlowJo 10.0.7.

Histological analysis of human synovial biopsy tissue

H&E stained sections of synovial biopsy tissue samples were scored for the severity of inflammatory infiltrate using the inflammatory component of the Krenn synovitis score[20]. Inflammatory infiltrates were graded from 0 to 3 (0=no inflammatory infiltrate, 1=few

Europe PMC Funders Author Manuscripts

mostly perivascular situated lymphocytes or plasma cells, 2=numerous lymphocytes or plasma cells sometimes forming follicle-like aggregates, and 3=dense band-like inflammatory infiltrate or numerous large follicle-like aggregates). Sections were scored by two blind individuals and then provided consensus.

Mice

All animal experiments were approved by the U.K. Home Office and conducted in accordance with the U.K.'s Animals (Scientific Procedures) Act 1986 and the U.K. Home Office Code of Practice. The project and experimental protocols were approved by the University of Birmingham Animal Ethics Review Committee who provided ethical oversight of the study.

C57BL/6 mice were purchased from Charles River and DBA/1 mice from Envigo. FAPα-DTR transgenic (Tg) embryos were a gift from Prof Douglas Fearon, generated as previously described[13]. ROSA$^{mT/mG}$ mice were purchased from Jackson laboratory and bred in the unit. All mice were housed at a barrier and specific pathogen-free facility at the Biomedical Services Unit, University of Birmingham. All mice used in experimental studies were male or females aged 8-10 weeks. Single animals were considered as experimental units.

In vivo imaging

FAPα-DTR mice were injected intra-peritoneally (i.p.) with 150μg/g body weight D-luciferin (PerkinElmer) and serially imaged using IVIS (Xenogen). The count data was normalised and expressed as radiance units of photons/second/cm^2/steradian (normalised bioluminescence) using Living Image software, version 4.7 (PerkinElmer) and presented as percentage change from baseline signal.

Diphtheria toxin mediated deletion of FAPα expressing cells

Diphtheria Toxin (DTx) (List Biological Laboratories) was administered by i.p. injection FAPα-DTR mice (25ng/g), twice a day, both in prophylactic (at day -7 and -5 pre STIA) and in therapeutic regimes (at days 3 and 5 or at days 5 and 7 or at days 10 and 12 post STIA). For the persistent inflammatory arthritis model, DTx injections (25ng/g) were performed on day 3 and day 5 initially and then once a week. For local deletion of FAPα$^+$ cells, DTx (5ng/g) was administrated by intra-articular (IA) injection into talo-tibial joint at day 4 and 6 post STIA. Sterile water for injections was used as vehicle control.

Mouse models of inflammatory arthritis

STIA was induced by intra-venous (i.v) injection of 100μl arthritogenic serum from KRN mice (K/BxN)[12]. Ankle or wrist joint thickness was monitored using callipers and reported as the change from baseline. In the persistent model of arthritis, mice were administered 100μl arthritogenic serum i.v. at day 0 and then 50μl once a week. Severity of joint swelling was quantified using the area under the curve (AUC) analysis of serial measurements.

For BrdU incorporation, mice were injected with 100μl of 10mg/ml BrdU in PBS and then kept on BrdU-containing drinking water (0.8mg/ml).

For collagen induced arthritis male DBA/1 mice were immunised with 100 or 200μg of rat CII emulsified 1:1 in complete Freund's adjuvant (CFA; Difco, containing *Mycobacterium butyricum*, 0.5 mg/ml) or Freund's incomplete adjuvant (IFA) containing *Mycobacterium tuberculosis* H37Ra (Difco; 3.33 mg/ml). Mice were boosted 3 weeks later with 100μg CII in IFA.

Mouse synovial tissue digestion

Bones with intact joints were dissected and transferred into RPMI-1640 (+2% FCS) containing 0.1g/ml Collagenase D (Roche), 0.01g/ml of DNase I (Sigma-Aldrich). Samples were incubated at 37°C, 40min, followed by incubation with medium containing 0.1g/ml Collagenase Dispase (Roche) and 0.01g/ml DNase I at 37°C for 20min.

Flow cytometry and cell sorting

Cells were stained at 4°C and dead cells excluded using Zombie Yellow staining (BioLegend). Peripheral blood was harvested by cardiac puncture into EDTA tubes, centrifuged and red cell lysis performed prior to staining. Antibodies used were anti-CD45 (30-F11), anti-THY1 (53-2.1), anti-podoplanin (8.1.1), Streptavidin APC (17-4317-82), anti-CD31 (390), anti-CD11b (M1/70), anti-SiglecF (1RNM44N), anti-CD11c (N418), anti-ITGA7 (334908), from eBioscience; anti-Ly-6G (1A8), anti-CD64 (X54-5/7.1), anti-F4/80 (BM8), anti-RANKL (IK22/5), anti-Ki67 (11F6), anti-CD140b (APB5), anti-CD146 (ME-9F1), anti-CD115 (AFS98), anti-CD43 (S11), anti-MHC Class II (39-10-8) and anti-Ly-6C (HK1.4), from BioLegend; anti-FAPα (R&D), mouse anti-goat/sheep IgG biotin (GT-34, Sigma Aldrich); and anti-BrdU (3D4, BD Biosciences). BrdU staining was performed according to manufacturer's instructions using a BrdU Flow Kit (BD Pharmigen™). CountBright™ absolute counting beads (Thermofisher) were used for analysis of cell numbers by flow cytometry, according to manufacturer's guidelines. Samples were acquired using a BD LSR Fortessa and analyzed by FlowJo, version 10.5.3. Cell sorting was performed immediately after staining using a MoFlo Astrios EQ machine (Beckman Coulter). For post sort populations purity was determined by re-analysis for the target population based on cell surface markers immediately post sorting. Purity was >99% for each target population.

Generation and analysis of droplet-based single cell RNA sequencing data

Following sorting, $CD45^-$ live synovial cells isolated from hind limbs of day 9 STIA inflamed mouse joints (n=3 biological replicate samples, each comprised of cells isolated from the joints of three animals) were captured with the 10X Genomics Chromium system. Sequencing libraries were generated using the 10x Genomics Single Cell 3' Solution (version 2) kit and subjected to Illumina sequencing (HiSeq 4000, read 2 sequenced to 75bp). Alignment, quantitation and aggregation of sample count matrices was performed using the 10x Genomics Cell Ranger pipeline (version 2.1.0) and mouse reference sequences (version 2.1.0), retaining a median of 59.9k reads/cell (mapped-read depth normalization applied). To circumvent known index-hopping issues with the HiSeq 4000 platform[21] cell barcodes common to more than one sample were removed from the aggregated count matrix. The UMI count matrix was randomly down-sampled to a common median number of per-cell counts between the samples. Downstream analysis was performed using the Seurat R

package (version 2.3.0)[16] as follows. Cells with greater than 5% mitochondrial reads or fewer than 500 genes were excluded from the analysis. Cells were down-sampled to a common number: for the full analysis we retained n=938 cells per replicate, while n=575 cells were retained per replicate for re-analysis of the fibroblasts. Per-cell counts were normalised, scaled and the effects of total UMI counts and percentage of mitochondrial counts regressed out. For the fibroblast re-analysis, the difference between G2M and S phase was also regressed out based on the expression of known cell cycle marker genes[22]. In both cases, we retained the first 30 principle components for tSNE projection and clustering analysis (original Louvain algorithm, resolution set to 0.6 for the full analysis and to 0.4 for the fibroblast reanalysis). Conserved cluster markers were identified as the intersection of those that were significant in separate tests of the cells from the each replicate (Wilcoxon test, Benjamini Hochberg (BH) adjusted p values < 0.1). Only genes found in 10% of cells (either within or outside the cluster of interest) and that showed a minimum log fold difference of 0.25 were tested for differential expression. Geneset over-representation analysis of cluster marker genes was performed using one-sided Fisher's exact tests (as implemented in the "gsfisher" R package https://github.com/sansomlab/gsfisher) with Biological Process gene sets obtained from the Gene Ontology (GO) database[23]. For this analysis cluster-specific gene universes were defined as those genes expressed in at least 10% percent of cells (either within or outside the cluster of interest). The computational analyses were performed using the "pipeline_cellranger.py" and "pipeline_seurat.py" pipelines (https://www.github.com/sansomlab/tenx/).

The diffusion map was generated using the "RunDiffusion" function in Seurat and the first 5 principal components. The pseudo-time tool Slingshot[14] was used to determine possible lineages via fitting of minimum spanning trees to the clusters (30 diffusion components, start cluster "F1"). The clusters and cluster markers from the human dataset[15] were obtained using the same workflow as described above (30 principal components and perplexity 100 for tSNE, resolution 0.6 for clustering). Only cells from RA patients and defined as fibroblasts by the authors were used in this analysis.

Bulk cell population RNA sequencing

For these studies, cells were isolated from the synovia of digested hind limb joints of day 9 STIA mice and analyzed by flow cytometry. After gating for fibroblasts (gating strategy outlined in extended data 1b) cells were sort purified into selected populations according to the sorting strategy in extended data 9a (each *n* number represents a single mouse with cells isolated from the joints of both hind limbs) and collected in EDTA free buffer. RNA was extracted from freshly isolated cells using the PicoPure RNA isolation kit (Thermo Fisher Scientific) according to the manufacturer's instructions. RNA quantity measured on the Qubit using the RNA HS kit (Invitrogen Q32852). Where samples were <5 ng/μl the Quantifluor RNA System was used (Promega E3310). cDNA synthesis was performed on isolated RNA using the SMART-Seq® v4 Ultra® Low Input RNA Kit for Sequencing (ClonTech 634890). Libraries were pooled and sequenced paired end 75 bases each end with the illumina NextSeq 500 system.

The reads were mapped to the GRCm38 (Ensemble release 85) mouse genome using STAR alignment software version v2.5.2b[24]. Read counts per gene were produced by the same software. Sample normalization and differential expression analysis was performed using DESeq2 R Bioconductor package[25]. log2 values of read counts regularised by DESeq2 were used in heatmaps in extended data 9. Gene set enrichment analysis was performed using GAGE R Bioconductor package[26] with gene sets from the Gene Ontology database.

Luminex analysis

Cells were stimulated with 1ng/ml recombinant mouse TNFα (Peprotech) *ex vivo* in culture medium for 1 hour. Fresh culture media was then applied and the subsequent supernatant was harvested after 12 hours and analysed using custom selected multiplex bead based assays (Luminex assay panel, RD).

Co-culture synovial fibroblasts-osteoclasts

Sorted synovial fibroblasts were cultured in DMEM (+10% FCS, +1% GPS). Bone marrow was flushed out from tibiae and femurs of 8-10 weeks old C57BL/6 or GFP mice and osteoclast precursors were cultured 24 hours in alpha-MEM (+10% FCS, +1% Glutamine-Penicillin-Streptomycin (GPS)). Supernatant from the bone marrow culture was removed (containing haematopoietic osteoclast precursors), cells were seeded on top of the fibroblast culture in alpha-MEM (+10% FCS, +1% GPS, 1μM prostaglandin E2, 10ng/ml recombinant TNFα). Experiment was stopped after 5 to 6 days in co-culture. Wells were imaged using Zeiss Observer Z1 microscope (ZEISS). GFP positive osteoclasts were counted using Zen 2010 software. Resorption area in wells of Osteo Assay surface plates were analysed using Adobe Photoshop, version 19.1.6, and ImageJ, version 1.51.

Quantitative real time PCR

RNA was isolated from single cell suspensions using the PicoPure RNA isolation kit (Thermo Fisher Scientific) according to manufacturer's instructions. For whole tissue analysis, frozen joints were pulverised in liquid nitrogen using a FreezerMill 6770 (Spex Sample Prep) and mRNA extracted using ReliaPrep™ RNA Tissue Miniprep System (Promega). cDNA synthesis was performed on all samples (500ng of RNA was transcribed) using iScript cDNA synthesis kit (Bio-Rad) on a Techne 312 thermal cycler PCR machine.

In order to amplify small amounts of cDNA without introducing amplification bias, TaqMan PreAmp Master Mix was used according to manufacturer's instructions for flow sorted cell samples.

Quantitative RT–qPCR was performed using Taqman assays and Taqman universal Mastermix (from Applied Biosystems) on a real-time PCR detection system (CFX96 Touch™ Real-Time PCR Detection System).

Expression levels were normalized to an internal housekeeping gene (RPLP0 for human, β-actin for mouse) and calculated as 2^–(CTHK–CTgene). TaqMan primer/probes (Applied Biosystems) used were *Fap* (human: Hs00990791_m1; mouse: Mm01329177_m1), *Pdpn* (Mm01348912_g1), *Thy1* (Mm00493681_m1), *CD34* (Mm00519283_m1), *CD248*

(Mm00547485_s1), *Cdh11* (Mm00515466_m1), *Pdgfra* (MM00440701_m1), *Vcam1* (Mm01320970_m1), *Ccl7* (Mm00443113_m1), *Csf2* (Mm01290062_m1), *Ccl2* (Mm00441242_m1), *Ccl5* (Mm01302427_m1), *Ccl8* (Mm01297183_m1), *Ccl9* (Mm00441260_m1), *Ccl11* (Mm00441238_m1), *Ccl19* (Mm00839967_g1), *Cxcl1* (Mm04207460_m1), *Cxcl2* (Mm00436450_m1), *Cxcl3* (Mm01701838_m1), *Cxcl5* (Mm00436451_g1), *Cxcl6* (Mm01302419_m1), *Cxcl11* (Mm00444662_m1), *Cxcl12* (Mm00445553_m1), *Cxcl13* (Mm04214185_s1), *Cxcl14* (Mm00444699_m1), *il18* (Mm00434226_m1), *Ptgs2* (Mm00478374_m1), *Ptges* (Mm00452105_m1), *Prg4* (Mm01284582_m1), *Tnfsf11* (Mm00441906_m1), *Mmp3* (Mm00440295_m1), *Mmp9* (Mm00442991_m1), *Mmp13* (Mm00439491_m1), *Ctsk* (Mm00484039_m1), *Runx2* (Mm00501584_m1), *Spp1* (Mm00436767_m1), *Acp5* (Mm00475698_m1), *Tnfrsf11a* (Mm00437132_m1), *Sost* (Mm00470479_m1), *BGLAP* (Mm03413826_mH), *Dmp1* (Mm01208363_m1), *il6* (Mm00446190_m1), *Tnf* (Mm00443258_m1), *il1b* (Mm00434228_m1), *il10* (Mm01288386_m1), *inos* (Mm00440502_m1) and *Arg1* (Mm00475988_m1).

Mouse tissue histology and immunofluorescence staining

Mouse legs were fixed for 24 hours in 10% formalin solution (Sigma-Aldrich) and decalcified in 10% EDTA (pH 7.4). Samples were embedded in paraffin, sectioned and H&E staining was performed at the Royal Orthopaedic Hospital Pathology Laboratories according to standard protocol. Safranin O staining for cartilage was performed as previously described[27].

Antigen retrieval was performed on FFPE tissue sections; 0.05% trypsin-EDTA for PDPN, FAPα and Cathepsin K staining at 37°C, or citrate buffer pH6 (Dako) at 58°C for F4/80 staining. Sections were stained with primary antibodies: anti-PDPN (eBio8.1.1, eBioscience), anti-FAPα (R&D), anti-F4/80 (BioRad), anti-CD146 (Abcam) or anti-Cathepsin K (Abcam). Secondary antibodies used were: biotin Goat anti-hamster IgG Antibody (BioLegend); biotin rabbit anti-sheep IgG (Vector Labs) biotin Goat anti-rabbit IgG (H+L) (Life Technologies); biotin rabbit anti-Rat IgG (H+L) (Vector Labs), followed by Streptavidin HRP and DAB detection or alkaline phosphatase, Vector Labs. Tissue sections were imaged using the AxioScanZ.1 slide scanner and analysed using Zen lite 2012 software. Quantification by pixel counts was performed using Image J, version 1.51.

For immunofluorescence, limbs were placed in a cryomold, embedded in OCT compound (both from Sakura Finetek) and stored at -80°C. Frozen sections were obtained with a tape transfer system CryoJane® (Leica Biosystems) and staining was performed on acetone-fixed sections with anti-PDPN (eBio8.1.1, Thermofisher), anti-FAPα (Abcam) and anti-THY1 (53-2.1, Thermofisher). The following secondary antibodies were used: Streptavidin Alexa Fluor™ 555, goat anti-rabbit IgG (H+L) FITC, Fluorescein/Oregon Green Polyclonal antibody AlexaFluor™ 488, goat anti-rat IgG (H+L) AlexaFluor™ 647, from Invitrogen; and biotin goat anti-hamster IgG (BioLegend). Images were acquired using a Zeiss LSM780 confocal microscope and ZEN pro 2011 imaging software.

Histomorphometry scoring

Analysis and cell counting of H&E and Safranin O was performed on images from whole joint tissue sections as previously described[28]. Leucocyte infiltration was scored 0-3 (0=normal, 1= minimal infiltration, 2=moderate infiltration, 3=marked infiltration). Osteoclasts were detected by both morphology and Cathepsin K staining. Scoring and measurements were performed by two independent blind assessors on a consistent region of the ankle joint and on three different cutting levels and expressed as a mean of these measurements.

Adoptive transfer of fibroblasts

500,000 live sort purified cells (from day 9 STIA) were injected into the inflamed talo-tibial joint at day 3 STIA recipient mice. Contralateral joint was injected with PBS. For CIA, cells were sort purified and injected into the ankle joint of DBA/1 mice with CIA at the first sign of arthritis, under the same experimental conditions described above.

Tracking of adoptively transferred cells *in vivo*

Cells were sort purified from digested synovia of day 9 STIA ROSA^{mTmG} mice and injected as described above. Harvested tissue was mounted in OCT, frozen, sectioned and fixed in acetone. For flow cytometry, sort purified cells were labelled with a cell trace dye (Invitrogen) according to the manufacturer's instructions prior to injection.

Micro-CT analysis

Hind limbs were imaged using a Skyscan 1172 micro-CT scanner (Bruker) using settings and reconstruction algorithms using MeshLab, version 1.3.2, as previously described[27]. Micro-CT meshes were divided into 3 regions: heel (compromising the calcaneus, centrale, distal tarsals, tibulae and astagalus and distal tibia and fibula), metatarsals and phalanges (excluding the claws). Each region was scored for erosion (0=normal, 1=roughness, 2=pitting, 3=full thickness holes) and the extent of the area affected (0=none, 1=a few small areas, 2=multiple small-medium areas, 3=multiple medium-large areas). The 2 scores were then multiplied together for each region. With the exception of local deletion and IA cell transfer studies, micro-CT scores from both the front and hind limb were combined as an average for each mouse.

Statistical analysis

Statistical analysis was performed as described in each section using Prism 8 software. Unless otherwise stated data is presented as Mean±SD from data obtained from at least two independent experiments. Parametric and non-parametric analyses were used where appropriate based on testing for a normal distribution using the D'Agostino-Pearson Omnibus normality test. Differences were considered to be significant when $p<0.05$. Multiple testing corrections were applied where appropriate.

Extended Data

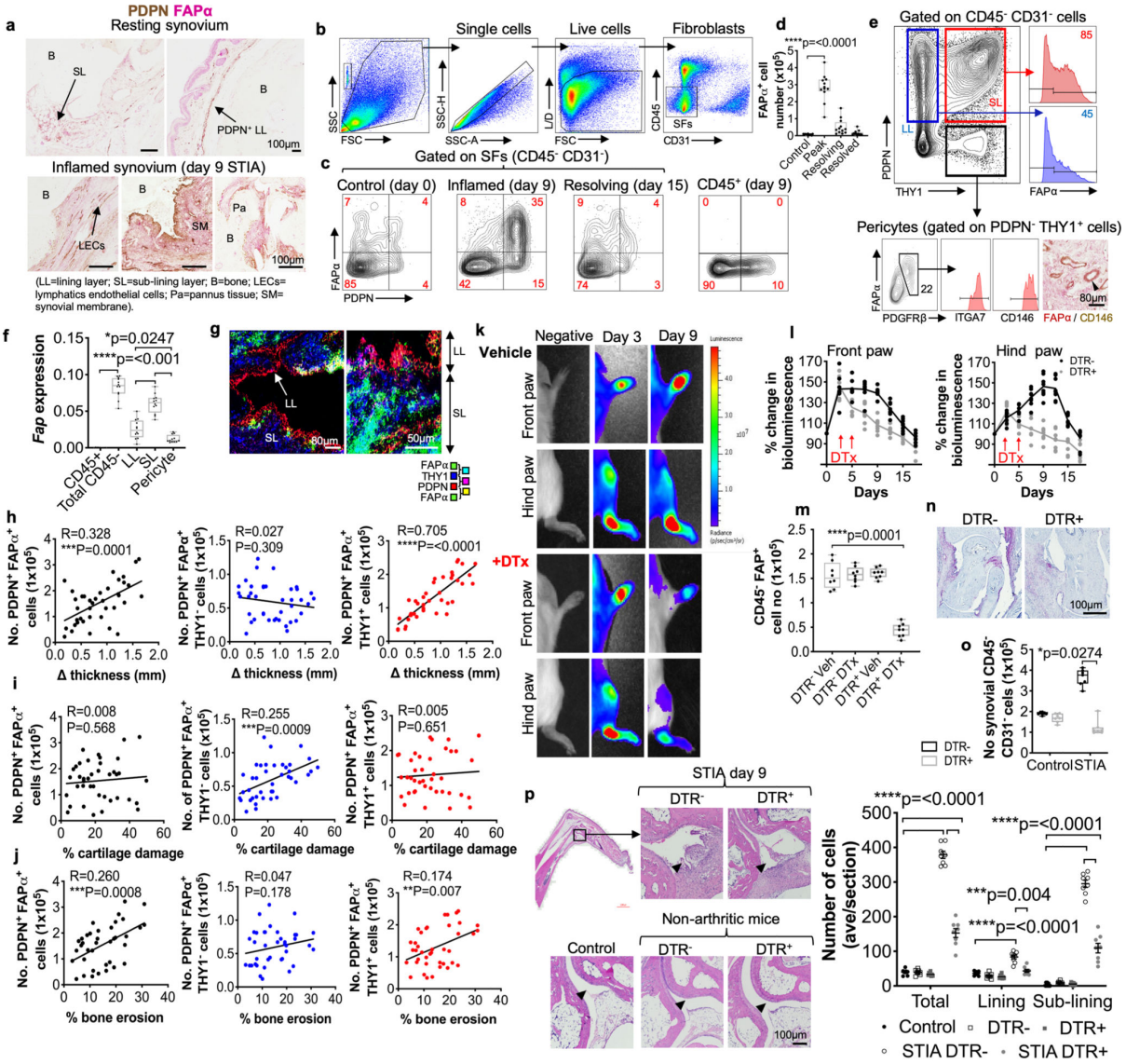

Extended data 1. Mouse synovial FAPα expression.

(**a**) Expression of PDPN and FAPα by immunohistochemistry in ankle joints (representative of n=8 mice). Flow cytometry of digested synovia: (**b**) gating strategy for SFs in digested synovia, (**c**) representative expression of PDPN and FAPα during STIA, (**d**) corresponding absolute numbers of FAPα$^+$ cells (n=10 mice per group), (**e**) plot of FAPα expression in THY1$^-$ (LL, blue) or THY1$^+$ (SL, red) PDPN$^+$ cells and PDPN$^-$ THY1$^+$ pericytes (black) in day 9 STIA synovia (each plot representative of n=12 mice, numbers=percentage of cells). (**f**) Quantification of *Fap* transcript expression in sort purified cells (day 9 STIA synovia, n=12 mice). (**g**) Immunofluorescence staining for PDPN, FAPα and THY1 expression in day 9 STIA ankle joints (representative of n=12 mice). Spearman's correlation analysis

Europe PMC Funders Author Manuscripts

between the total (black), LL (blue) and SL (red) FAPα expressing cells quantified by flow cytometry and (**h**) the change in ankle joint thickness, (**i**) cartilage destruction and (**j**) bone erosion (both by histology) (n=40 mice). (**k**) Representative bioluminescence of *in vivo* imaging of FAPα-DTR^{+} mice treated with DTx or Vehicle and (**l**) quantification of bioluminescence (n=8 mice per group). (**m**) Quantification of synovial FAPα^{+} cells following administration of either DTx or Vehicle (n=8 mice per group). (**n**) Immunohistochemistry staining of FAPα (red) expression in ankle joints following DTx (representative of n=8 mice). (**o**) Total number of CD45^{-} CD31^{-} cells by flow cytometry in day 9 STIA synovia compared to non-arthritic (control) mice following DTx (n=7 mice per group). (**p**) H&E staining and quantification of cellularity following DTx treatment. Arrow indicates SM. Data are expressed as the average number of cells per quantified per histological section (n=8 mice per group). Statistics: 2-way ANOVA with Tukey's post hoc, (**f,n,p**). Data represented as Mean±S.D., except **f,n** which are shown as box plots (centre line, median; box limits, upper and lower quartiles; whiskers, maximum and minimum values.

Europe PMC Funders Author Manuscripts

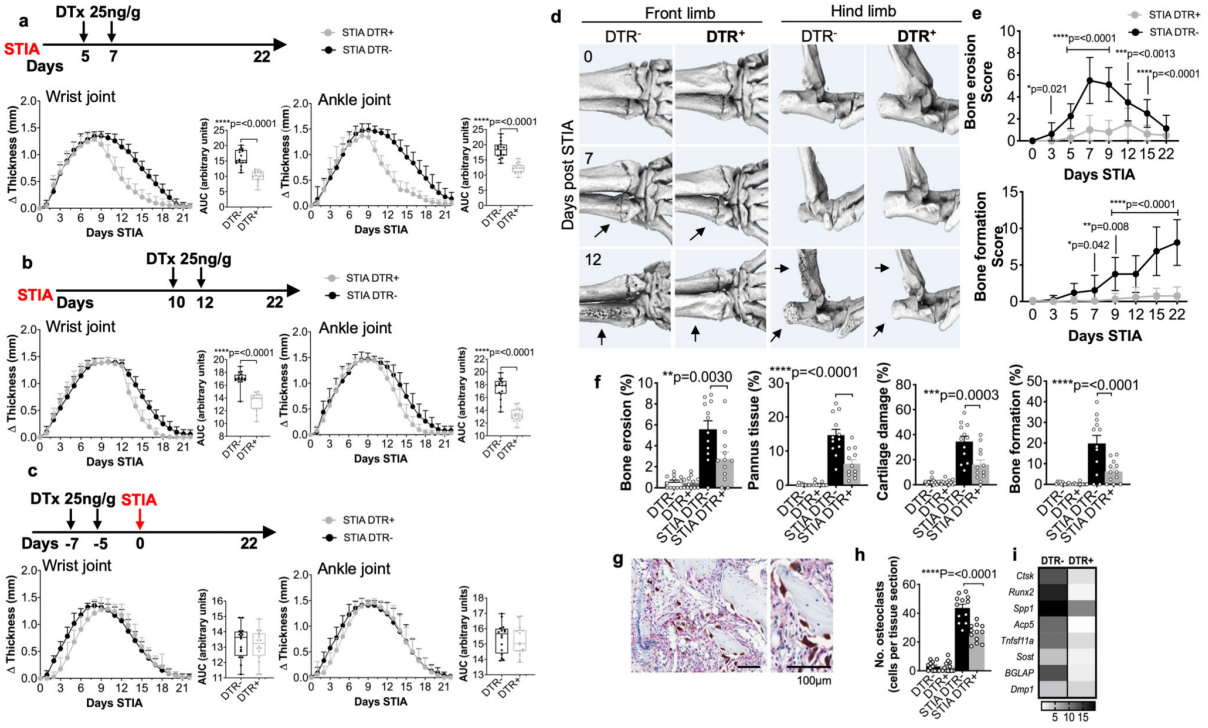

Extended data 2. Effects of FAPα cell deletion.

Change in wrist and ankle joint thickness during STIA with AUC analysis following FAPα cell deletion at (**a**) days 5 and 7 and (**b**) days 10 and 12 or (**c**) prophylactically prior to the induction of STIA (n=8, mice per group). (**d**) Representative time course analysis of structural joint damage assessed by micro-CT following FAPα cell deletion at days 3 and 5 following induction of STIA, with (**e**) quantification of bone erosion and new bone formation (n=8 mice per group), combined for front and hind paws. (**f**) Histological examination of ankle joint tissue sections at day 12 STIA with quantification of bone erosion, pannus formation and bone formation (all by H&E) and cartilage destruction (by Safranin O staining) (n=12 mice per group). (**g**) Representative images of cathepsin k immunohistochemical staining of osteoclasts (brown) in the ankle joints of day 12 STIA mice. (**h**) Number of osteoclasts (cathepsin k positive) per tissue section in DTR^- versus DTR^+ mice at day 12 STIA compared to non-arthritic control mice (n=12 mice per group). (**i**) Expression of bone turnover markers including osteoclast and osteoblast markers in whole paw tissue analysed by RT-PCR (n=8 mice per group, data are expressed as mean fold change in expression compared to expression in non-arthritic mice). Statistics: Mann Whitney test, **a-c**, 2-way ANOVA with Tukey's post hoc, **e**, 1-way ANOVA with Tukey's post hoc, **f,h**. Data represented as Mean±S.D., except AUC analysis in **a-c** which are shown as box plots (centre line, median; box limits, upper and lower quartiles; whiskers, maximum and minimum values.

Europe PMC Funders Author Manuscripts

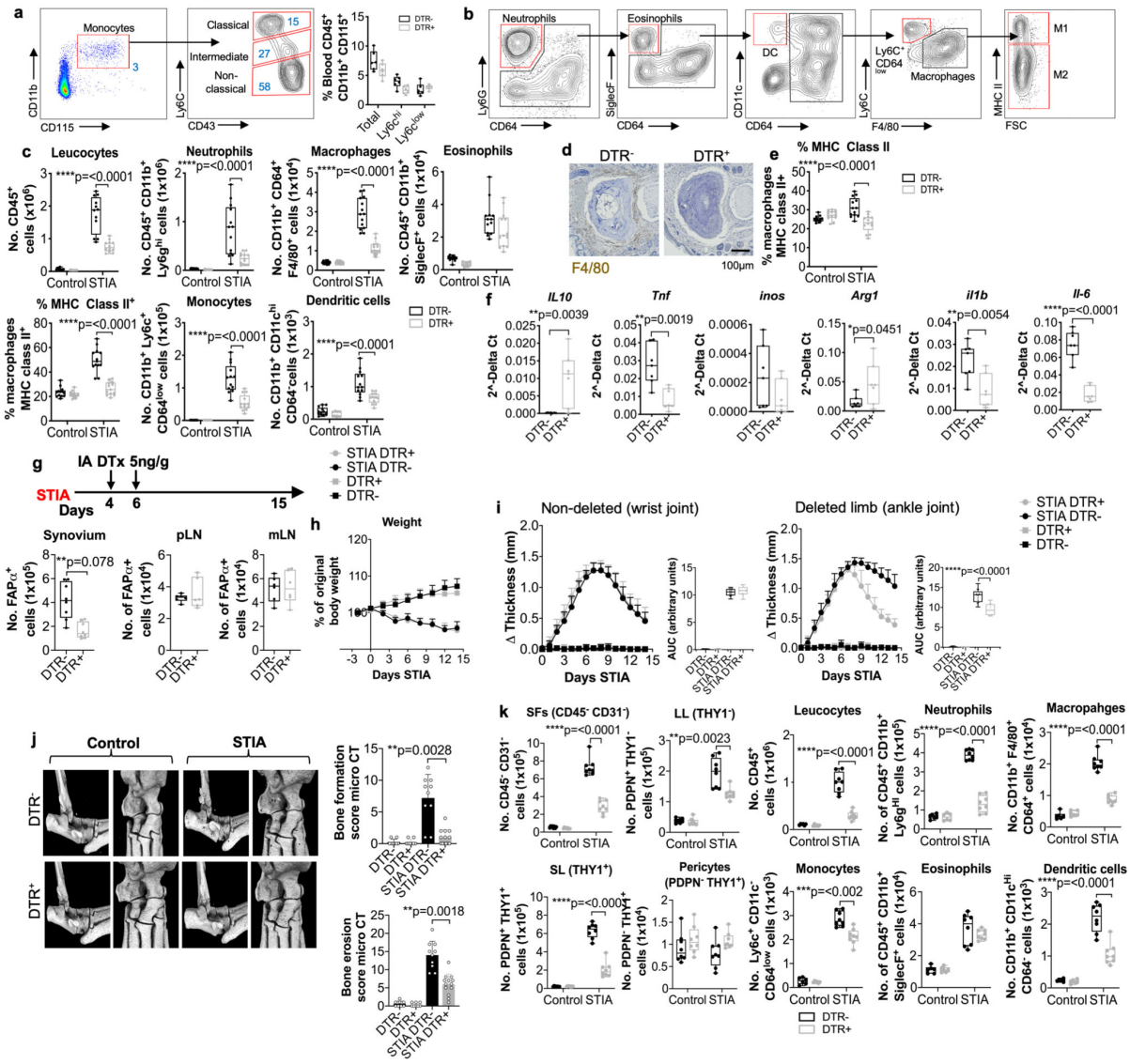

Extended data 3. Effect of FAPα cell deletion on leucocyte infiltration.

(**a**) Flow cytometry plot of peripheral blood monocytes (numbers=percentage of positive cells) with quantification at day 9 STIA following DTx at day 3 and day 5 (n=6 mice per group). (**b**) Flow cytometry gating strategy for leucocyte populations in digested synovia. (**c**) Numbers of leucocytes and percentage of MHC Class II expressing F4/80 cells (M1) in hind limb joints of day 28 persistent STIA mice analysed by flow cytometry (n=13 mice per group). (**d**) Representative immunohistochemical staining of macrophages (F4/80$^+$, brown; nuclei blue) in the ankle joint tissue sections at day 12 STIA mice following DTx at day 3 and 5 (representative of n=6 mice). (**e**) Percentage of F4/80$^+$ macrophages staining positive for MHC Class II as detected by flow cytometry in day 12 STIA digested synovia from DTR

Europe PMC Funders Author Manuscripts

Europe PMC Funders Author Manuscripts

$^{+/-}$ mice following DTx at day 3 and 5 (n=13 mice per group). (**f**) Expression of functional macrophage markers detected by RT-PCR in sort purified macrophages ($CD45^+$ $CD11b^+$ $F4/80^+$) isolated from the synovia of day 12 STIA mice following DTx at day 3 and 5 (n=7 mice per group). (**g**) Number of FAPα expressing cells quantified by flow cytometry from digested synovia (n=8 mice), popliteal (draining) and mesenteric (non-draining) lymph nodes (n=6 mice) following IA administration of DTx into the ankle joint during STIA (harvested day 14) and (**h**) daily change in weight from baseline (expressed as percentage of original body weight) in STIA mice compared to non-arthritic mice (n=6 mice). (**i**) Effect of local deletion of synovial FAPα expressing cells (by IA injection of DTx); on ankle joint thickness in the resolving model of STIA model when compared to the wrist joints on the same mouse (non-deleted limbs) (n=8 mice) and to non-arthritic DTR+ and DTR- injected mice (n=6 mice per group) with AUC analysis. (**j**) Representative micro-CT images of day 14 STIA and non-arthritic control mice following IA injection of DTx and quantification of bone erosion and new bone formation (STIA DTR^- n=10, STIA DTR^+ n=13, DTR^- and DTR^+ n=8). (**k**) Quantification of the number of fibroblasts and leucocytes in digested synovia of day 9 STIA mice analysed by flow cytometry following IA administration of DTx (n=8 mice). Statistics: 2-way ANOVA with Tukey's post hoc **a,c,e,h,k**, two-tailed paired Student's t-test, **f,g**, 1-way ANOVA with Tukey's multiple comparison tests, **I,j**. Data represented as Mean±S.D., except **a,c,e,f,g,k** and AUC analysis in **I,** which are shown as box plots (centre line, median; box limits, upper and lower quartiles; whiskers, maximum and minimum values.

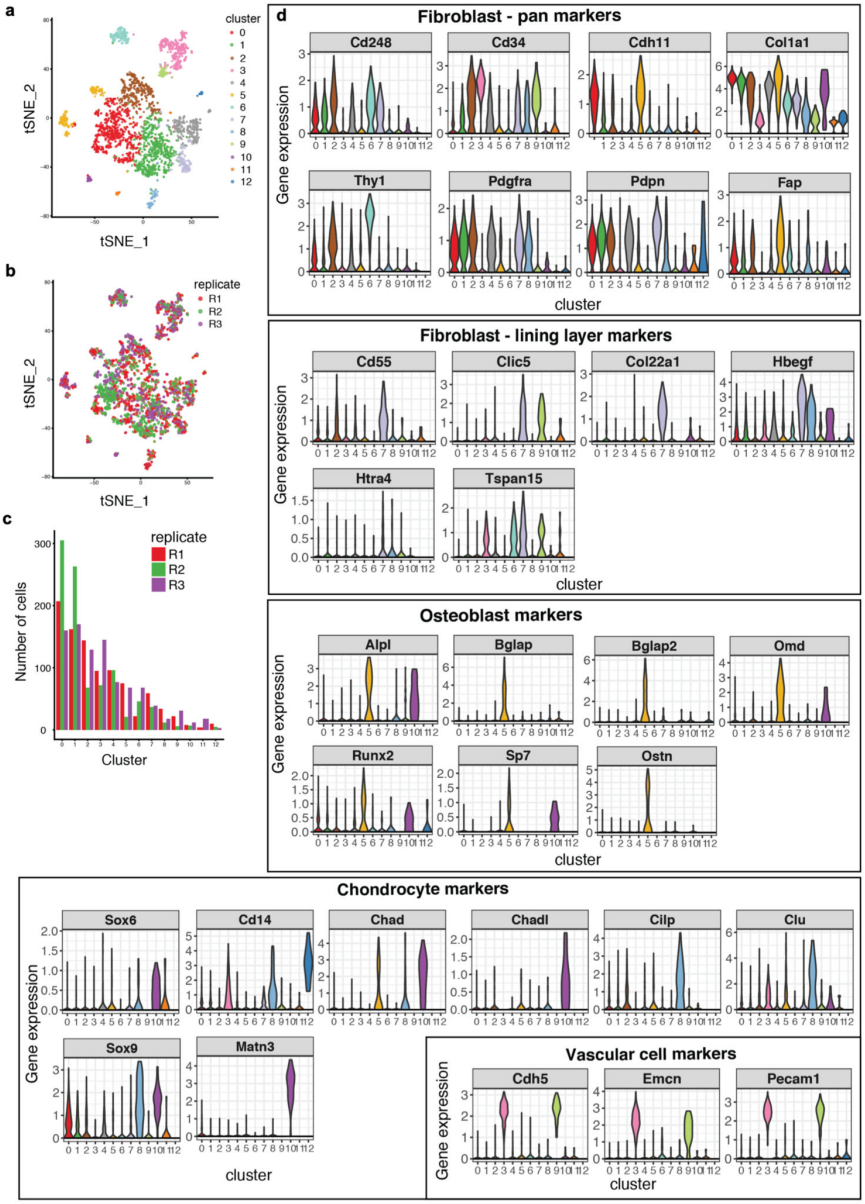

Extended data 4. 10x Chromium single cell RNAseq (droplet based single cell) analysis of CD45$^-$ cell populations from inflamed synovium.

(**a**) t-SNE projection of non-hematopoietic stromal cells from the inflamed mouse joint (n=3 biological replicates, day 9 STIA) showing the initial automatic cluster assignments from Seurat (projection is identical to that shown in Fig 3a). (**b**) The same t-SNE plot coloured for biological replicate. (**c**) The barplot shows the number of cells in each cluster stratified by replicate. (**d**) **Cluster cell identification:** the five panels of violin plots show expression (normalised, log-transformed counts of the cells from all of the n=3 biological replicates, y

axes) of known cell type marker genes (for fibroblasts, lining layer fibroblasts, osteoblasts, chondrocytes, and vascular cells) in each of the automatically assigned clusters (x axes). The colours of violin plots correspond to those shown in **Extended data Data 4a**.

Europe PMC Funders Author Manuscripts

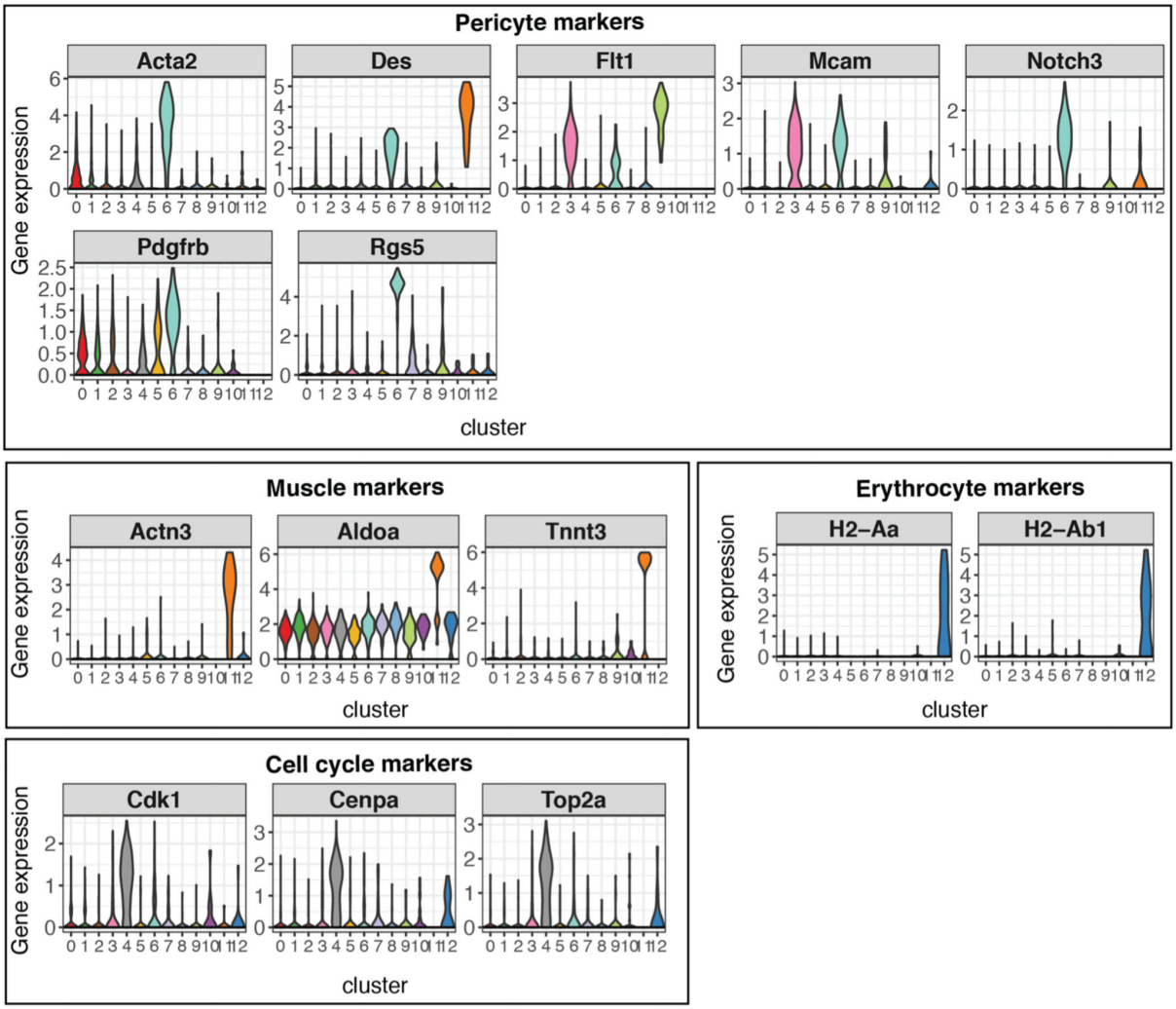

Extended data 5. continued cluster identification analysis.

The four panels of violin plots show expression (normalised, log-transformed counts of the cells from all of the n=3 biological replicates, y axes) of known cell type marker genes (for pericytes, muscle cells, erythrocytes and the cell cycle) in each of the automatically assigned clusters (x axes). The colours of violin plots correspond to those shown in Extended data 4a.

Europe PMC Funders Author Manuscripts

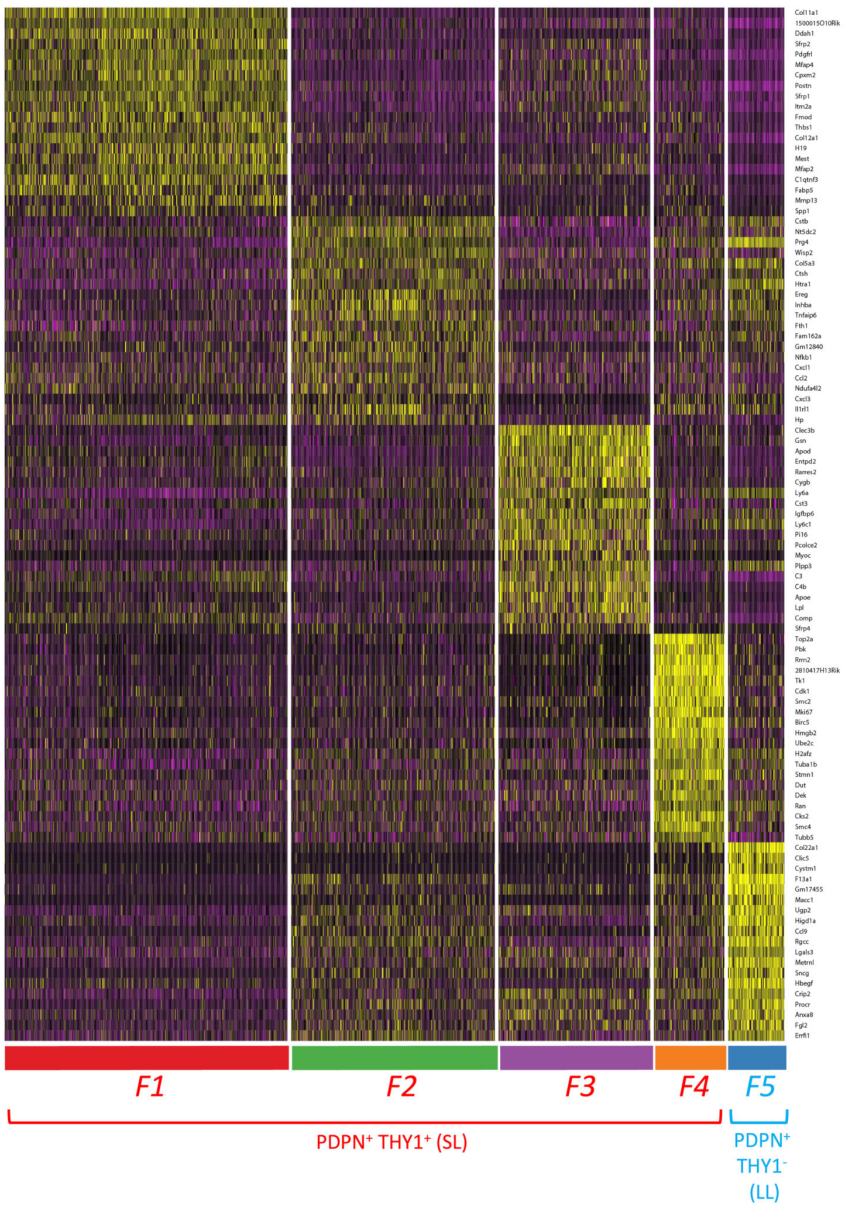

Extended data 6. Differential gene expression between fibroblast clusters.

The heat map shows the (row-scaled) expression of the top 20 (by p-value) discovered significant, conserved marker genes for each cluster (BH adjusted p-value <0.1 in separate tests of cells from each of the n=3 biological replicate samples, two-sided Wilcoxon tests). Each column represents a single fibroblast and each row the given gene. The cluster identification is indicated for each column. LL: lining layer fibroblasts correspond to F5 and are PDPN^{+} THY1^{-} and SL: sub-lining layer fibroblasts correspond to F1-F4 fibroblast subsets and are PDPN^{+} THY1^{-}.

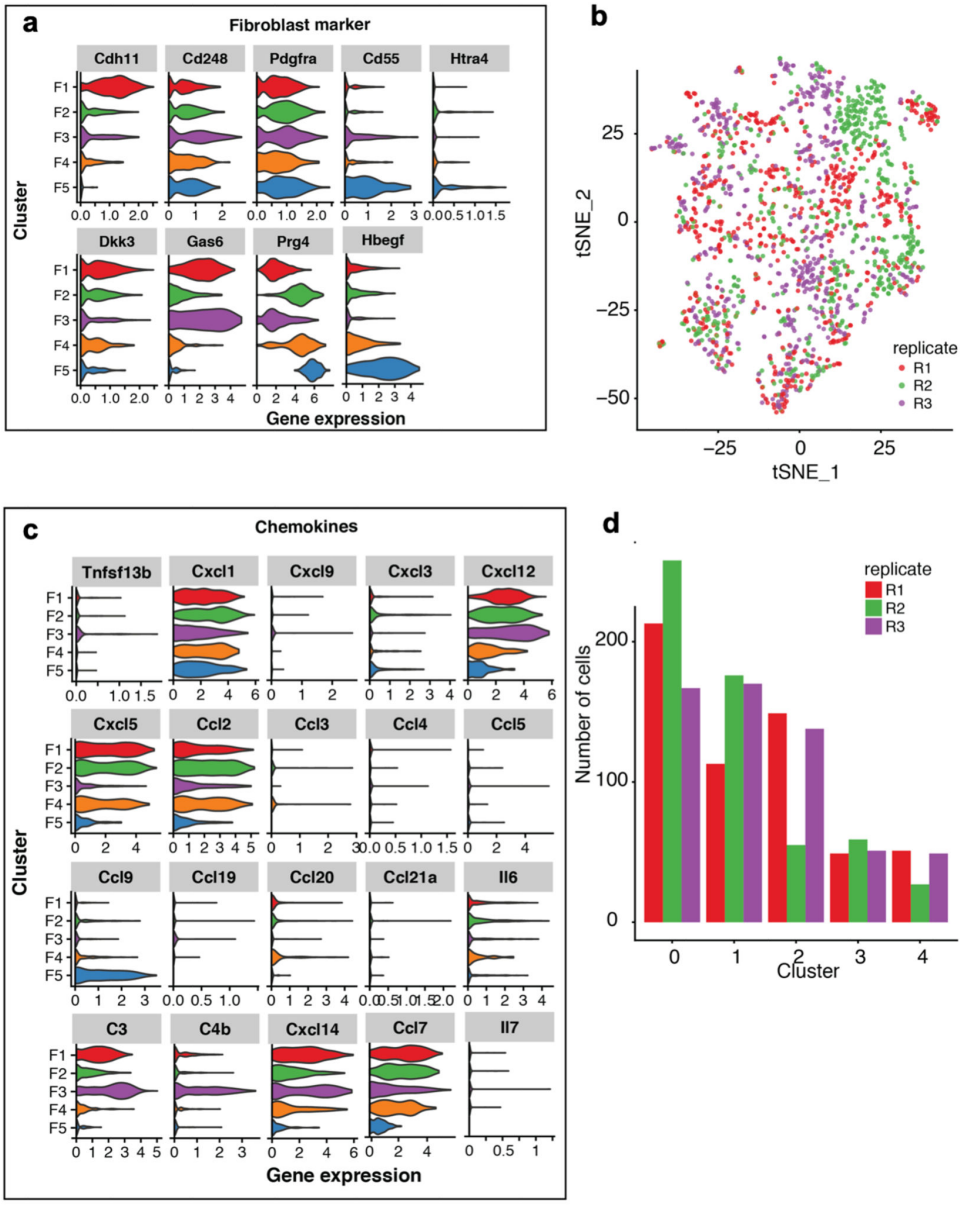

Extended data 7. Differential gene expression in specific fibroblast clusters.

(**a**) A set of violin plots showing gene expression (normalised, log-transformed counts of the cells from all of the n=3 biological replicates, x axes) of additional fibroblast markers in each of the F1-F5 fibroblast clusters (y axes) (corresponds to Fig 3b). (**b**) t-SNE projection of fibroblasts from the inflamed mouse joint coloured by replicate (corresponds to Fig 3b). (**c**) A set of violin plots showing gene expression (normalised, log-transformed counts of the cells from all of the n=3 biological replicates, x axes) of known markers for chemokines in

each of the F1-F5 fibroblast clusters (y axes) (corresponds to Fig 3B). (**d**) Number of cells in each cluster stratified by replicate.

Europe PMC Funders Author Manuscripts

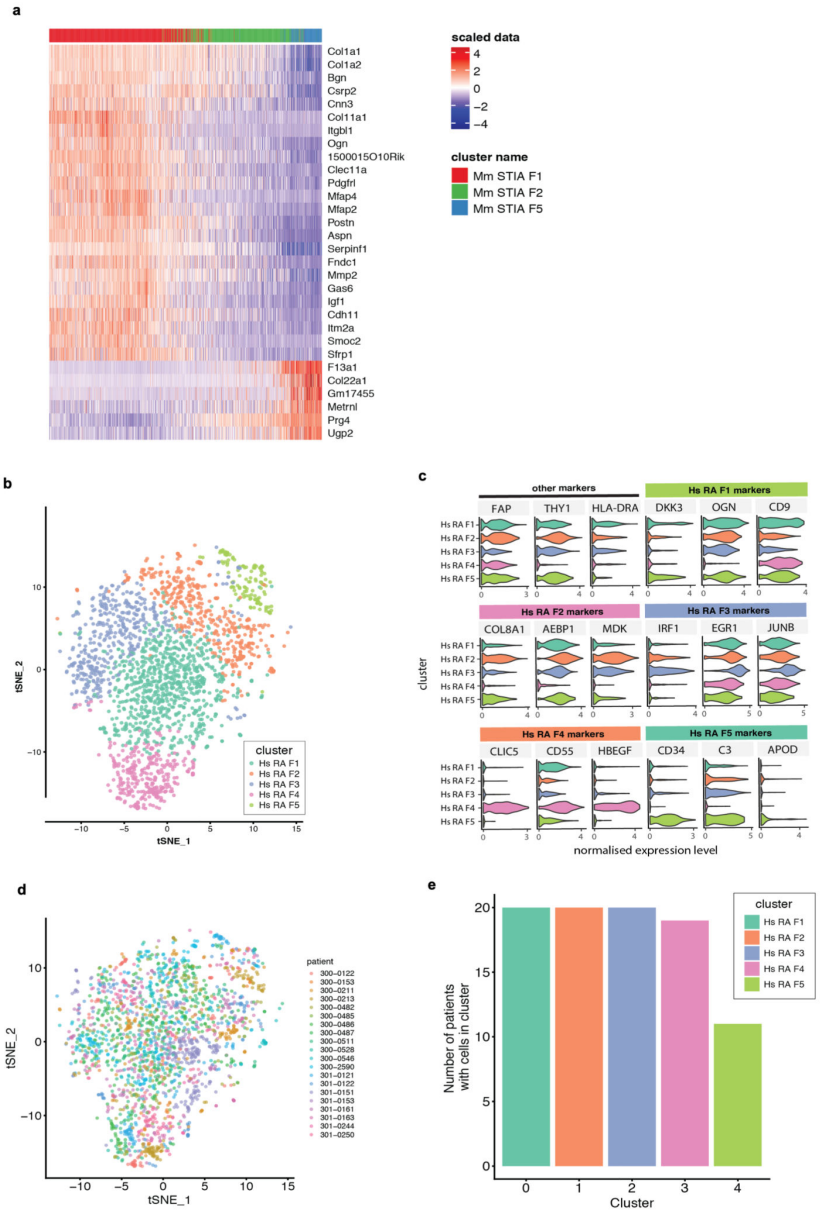

Extended data 8. Trajectory analysis and identification of fibroblast subpopulations from human RA patients.

(**a**) The Heatmap shows genes most strongly up- or downregulated across the inferred F1-F2-F5 trajectory in the mouse fibroblasts from the STIA model (as determined by Slingshot[14]). **(b-e)** Re-analysis of CEL-Seq2 single-cell RNA-sequencing dataset from 20 RA patients[15]. (**b**) t-SNE projection of the RA patient fibroblasts indicating the automatic cluster assignments from Seurat. (**c**) The sets of violin plots show expression (normalised, log-transformed counts, cells from all n=20 RA patients, x axes) of cluster marker genes in

each of the RA patient fibroblast clusters (y axes). The violin plots are grouped into six sets comprising of 'other markers' (known markers or markers reported by Zhang et al[15]) or of markers characteristic of each of the Hs RA F1-F5 clusters as indicated. (**d**) The same t-SNE plot as in (**a**) coloured by patient ID. (**e**) The barplot shows the number of patients represented in each assigned cluster.

Europe PMC Funders Author Manuscripts

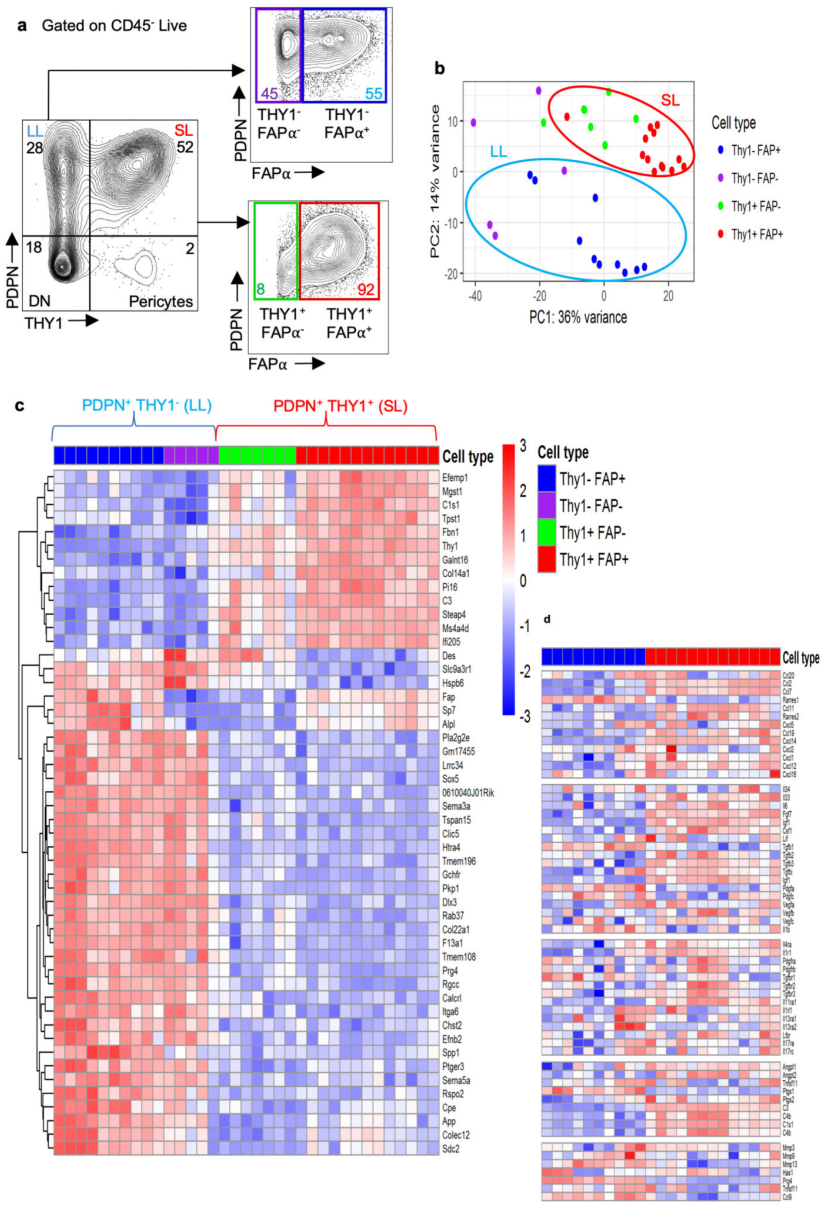

Extended data 9. Bulk RNA sequencing of sort purified FAPα expressing LL and SL cell populations from the inflamed hind limb joints of day 9 STIA mice.

(**a**) Gating strategy for flow cytometry based cell sorting from day 9 STIA digested synovia gated on CD45- CD31- live cells. Coloured gates correspond to each sort purified population and the percentage gated cell population is indicated. (**b**) Principal components analysis (PCA) reveals each population clusters according to either a SL phenotype or a LL phenotype. Each dot presents a single biological replicate sample and is coloured according to the gating strategy outlined in (**a**). (**c**) The heat map shows the differential expression of

the 50 most significant genes (by p value) for each population (BH adjusted p-value <0.1) and reveals distinct transcriptional profiles between $THY1^+$ and $THY1^-$ cell populations. (**d**) Expression of specific genes RNA sequencing in $PDPN^+$ $FAP\alpha^+$ $THY1^-$ versus $PDPN^+$ $FAP\alpha^+$ $THY1^+$ sort purified cells. For each heatmap a column represents a single biological replicate and coloured according to the gating strategy in (**a**). Biological replicates represent cells isolated and purified from the digestion of synovia from the hind limbs of a single mouse (n=10 $THY1^-$ $FAP\alpha^+$, n=5 $THY1^-$ $FAP\alpha^-$, n=6 $THY1^+$ $FAP\alpha^-$ and n=12 $THY1^+$ $FAP\alpha^+$ samples).

Europe PMC Funders Author Manuscripts

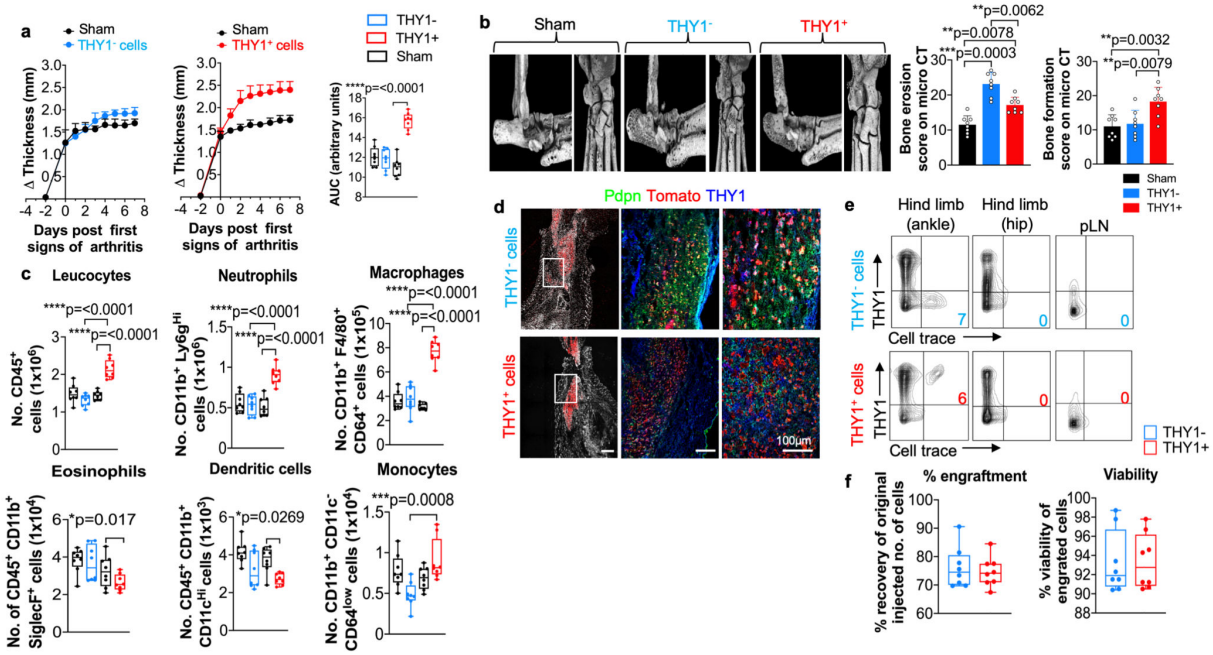

Extended data 10. Effect of IA injection of fibroblast subsets.

(**a**) Effect on ankle joint thickness of IA injection of 500,000 sort purified PDPN$^+$ FAPα$^+$ THY1$^-$ (blue) or PDPN$^+$ FAPα$^+$ THY1$^+$ (red) cells into the ankle joint of CIA mice at the first sign of joint inflammation (day 0) compared to contralateral sham injected joints (n=8 mice per group). (**b**) Representative images of micro-CT analysis and quantification of bone erosion and new bone formation (n=8 mice per group). (**c**) Flow cytometric analysis of leucocytes in the digested synovia of injected joints, 7 days post injection (n=8 mice per group). (**d**) Representative confocal microscopy of ankle joint tissue of mice injected with red Tomato expressing PDPN$^+$ FAPα$^+$ THY1$^-$ or PDPN$^+$ FAPα$^+$ THY1$^+$ isolated from day 9 STIA cells and injected into day 3 STIA recipient mice (representative images from n=6 mice, 14 days post injection). (**e**) Flow cytometric analysis of digested synovia, 14 days post injection of cell trace labelled cells (isolated from day 9 STIA mice and injected into the ankle joint of day 3 STIA recipient mice), gated on the CD45$^-$ CD31$^-$ PDPN$^+$ cell fraction. Percentage of THY1$^+$ (red) or THY1$^-$ (blue) cell in this gated cell fraction is indicated (representative of n=6 per group). (**f**) Percentage of engraftment and viability of injected cells 14 days post injection into the ankle joints of STIA mice (n=8 per treatment group, two tailed Student's t-test). Engraftment is expressed as the percentage recovery of the original injected cell number. Statistics: 1-way ANOVA with Bonferroni post hoc test, **b,c** and AUC analysis **a**. Paired two-tailed Student's t-test **f**. Data represented as Mean±S.D., except **c,e** and AUC analysis in **a,** which are shown as shown as box plots (centre line, median; box limits, upper and lower quartiles; whiskers, maximum and minimum values.

Supplementary Material

Refer to Web version on PubMed Central for supplementary material.

Europe PMC Funders Author Manuscripts

Acknowledgements

APC was supported by a Wellcome Trust clinical career development fellowship #WT104551MA; AF by Arthritis Research UK clinician scientist fellowship #18547; FB by an Arthritis Research UK senior fellowship; CW was supported by a Deutsche Forschungsgemeinschaft (DFG) Fellowship (Ref 319464273). KW by Rheumatology Research Foundation Scientist Development Award; KJ by a Wellcome Trust PhD studentship; SNS and MA are supported by the Kennedy Trust for Rheumatology Research. This work was supported by the Arthritis Research UK Rheumatoid Arthritis Pathogenesis Centre of Excellence #20298 (RACE); The National Institutes of Health Accelerating Medicines Partnership in RA/SLE and Arthritis Research UK programme grant #19791 (to CDB). This paper presents independent research supported by the NIHR Birmingham Biomedical Research Centre at the University Hospitals Birmingham NHS Foundation Trust and the University of Birmingham. The views expressed are those of the author(s) and not necessarily those of the NHS, the NIHR, our funding bodies or the Department of Health.

References

1. Baker KF, Isaacs JD. Novel therapies for immune-mediated inflammatory diseases: What can we learn from their use in rheumatoid arthritis, spondyloarthritis, systemic lupus erythematosus, psoriasis, Crohn's disease and ulcerative colitis? Ann Rheum Dis. 2018; 77:175–187. [PubMed: 28765121]
2. Smolen JS, Aletaha D. Rheumatoid arthritis therapy reappraisal: strategies, opportunities and challenges. Nat Rev Rheumatol. 2015; 11:276–289. [PubMed: 25687177]
3. Croft AP, et al. Rheumatoid synovial fibroblasts differentiate into distinct subsets in the presence of cytokines and cartilage. Arthritis Res Ther. 2016; 18:270. [PubMed: 27863512]
4. Mizoguchi F, et al. Functionally distinct disease-associated fibroblast subsets in rheumatoid arthritis. Nat Commun. 2018; 9:789. [PubMed: 29476097]
5. Stephenson W, et al. Single-cell RNA-seq of rheumatoid arthritis synovial tissue using low-cost microfluidic instrumentation. Nat Commun. 2018; 9:791. [PubMed: 29476078]
6. Gerlag DM, Norris JM, Tak PP. Towards prevention of autoantibody-positive rheumatoid arthritis: from lifestyle modification to preventive treatment. Rheumatology. 2016; 55:607–614. [PubMed: 26374913]
7. Pap T, Müller-Ladner U, Gay RE, Gay S. Fibroblast biology. Role of synovial fibroblasts in the pathogenesis of rheumatoid arthritis. Arthritis Res. 2000; 2:361–367. [PubMed: 11094449]
8. Ospelt C, Gay S. The role of resident synovial cells in destructive arthritis. Best Pract Res Clin Rheumatol. 2008; 22:239–252. [PubMed: 18455682]
9. McGettrick HM, Butler LM, Buckley CD, Rainger GE, Nash GB. Tissue stroma as a regulator of leukocyte recruitment in inflammation. J Leukoc Biol. 2012; 91:385–400. [PubMed: 22227966]
10. Choi IY, et al. Stromal cell markers are differentially expressed in the synovial tissue of patients with early arthritis. PLoS ONE. 2017; 12:e0182751. [PubMed: 28793332]
11. Filer A. The fibroblast as a therapeutic target in rheumatoid arthritis. Curr Opin Pharmacol. 2013; 13:413–419. [PubMed: 23562164]
12. Kollias G, et al. Animal models for arthritis: innovative tools for prevention and treatment. Ann Rheum Dis. 2011; 70:1357–1362. [PubMed: 21628308]
13. Roberts EW, et al. Depletion of stromal cells expressing fibroblast activation protein-α from skeletal muscle and bone marrow results in cachexia and anemia. J Exp Med. 2013; 210:1137–1151. [PubMed: 23712428]
14. Street K, et al. Slingshot: cell lineage and pseudotime inference for single-cell transcriptomics. BMC Genomics. 2018; 19:477. [PubMed: 29914354]
15. Zhang F, et al. Defining Inflammatory Cell States in Rheumatoid Arthritis Joint Synovial Tissues by Integrating Single-cell Transcriptomics and Mass Cytometry. bioRxiv. 2018; 351130doi: 10.1101/351130
16. Butler A, Hoffman P, Smibert P, Papalexi E, Satija R. Integrating single-cell transcriptomic data across different conditions, technologies, and species. Nat Biotechnol. 2018; 36:411–420. [PubMed: 29608179]

17. Aletaha D, et al. 2010 Rheumatoid arthritis classification criteria: An American College of Rheumatology/European League Against Rheumatism collaborative initiative. Arthritis Rheum. 2010; 62:2569–2581. [PubMed: 20872595]
18. Filer A, et al. Identification of a transitional fibroblast function in very early rheumatoid arthritis. Ann Rheum Dis. 2017; 76:2105–2112. [PubMed: 28847766]
19. Donlin LT, et al. High dimensional analyses of cells dissociated from cryopreserved synovial tissue. 2018; doi: 10.1101/284844
20. Krenn V, et al. Synovitis score: discrimination between chronic low-grade and high-grade synovitis. Histopathology. 2006; 49:358–364. [PubMed: 16978198]
21. Sinha R, et al. Index Switching Causes 'Spreading-Of-Signal' Among Multiplexed Samples In Illumina HiSeq 4000 DNA Sequencing. 2017; doi: 10.1101/125724
22. Tirosh I, et al. Single-cell RNA-seq supports a developmental hierarchy in human oligodendroglioma. Nature. 2016; 539:309–313. [PubMed: 27806376]
23. Ashburner M, et al. Gene ontology: tool for the unification of biology. The Gene Ontology Consortium. Nat Genet. 2000; 25:25–29. [PubMed: 10802651]
24. Dobin A, et al. STAR: ultrafast universal RNA-seq aligner. Bioinformatics. 2013; 29:15–21. [PubMed: 23104886]
25. Love MI, Huber W, Anders S. Moderated estimation of fold change and dispersion for RNA-seq data with DESeq2. Genome Biol. 2014; 15:550. [PubMed: 25516281]
26. Luo W, Friedman MS, Shedden K, Hankenson KD, Woolf PJ. GAGE: generally applicable gene set enrichment for pathway analysis. BMC Bioinformatics. 2009; 10:161. [PubMed: 19473525]
27. Ross EA, et al. Treatment of inflammatory arthritis via targeting of tristetraprolin, a master regulator of pro-inflammatory gene expression. Ann Rheum Dis. 2016; doi: 10.1136/annrheumdis-2016-209424
28. Wehmeyer C, et al. Sclerostin inhibition promotes TNF-dependent inflammatory joint destruction. Sci Transl Med. 2016; 8:330ra35–330ra35.

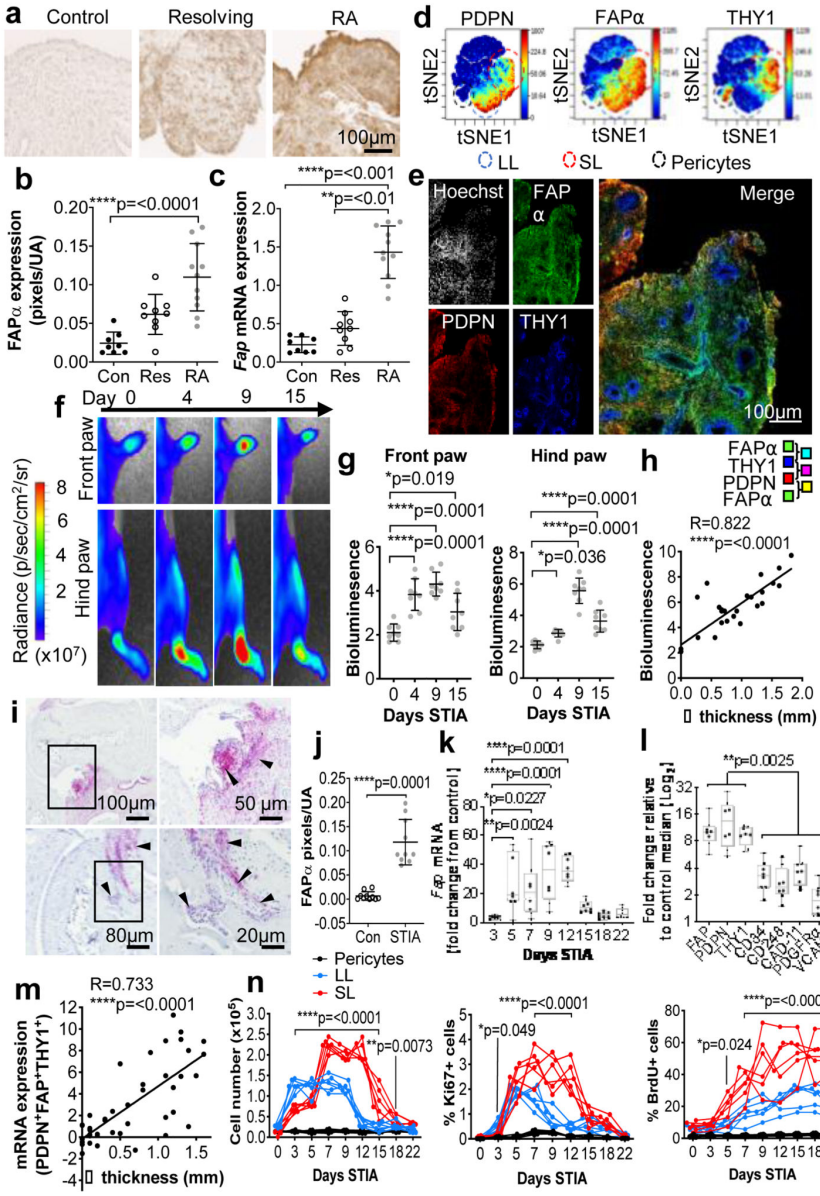

Fig. 1. FAPα^{+} SFs accumulate in the arthritic joint.

(**a**) Representative images of FAPα expression in synovial tissue and (**b**) quantification, with (**c**) matched *Fap* transcript expression in SFs expanded *in vitro* (n=8 control, 9 resolving and 11 RA, patient samples). (**d**) CyToF viSNE plots of CD45^{-} cells and (**e**) confocal microscopy of RA synovium (both representative of n=8, RA patient samples). (**f**) Serial measurements of bioluminescence signal in FAPα-luciferase mice and (**g**) quantification during STIA (n=8 mice). (**h**) Spearman's correlation between bioluminescence and joint thickness (n=30 mice). (**i**) Representative image of FAPα (red) expression in hind limb

joints of day 9 STIA mice, arrows indicate FAPα expression and (**j**) quantification (n=10 mice per group). (**k**) *Fap* transcript expression in sort purified synovial CD45$^-$ CD31$^-$ cells during STIA (n=8 mice, per time point). (**l**) Fold change in mRNA expression of stromal markers in the synovia of day 9 STIA compared to control mice (n=8 mice). (**m**) Spearman's correlation between combined expression of *Pdpn*, *Thy1* and *Fap,* and ankle joint thickness (n=44 mice). (**n**) Change in absolute numbers and percentage of Ki67$^+$ and BrdU$^+$ cells during STIA (n=6 mice). Statistics: Kruskal-Wallis with Dunn's post-hoc, **b,c**, 1-way ANOVA with Dunnett's post hoc, compared to day 0, **g** or day 3 **k**, two-tailed Mann-Whitney test **j**, 2-way ANOVA with Tukey's post hoc, **l,n**. Data represented as Mean±S.D., except **g,k,l,** which are shown as box plots (centre line, median; box limits, upper and lower quartiles; whiskers, maximum and minimum values).

Europe PMC Funders Author Manuscripts

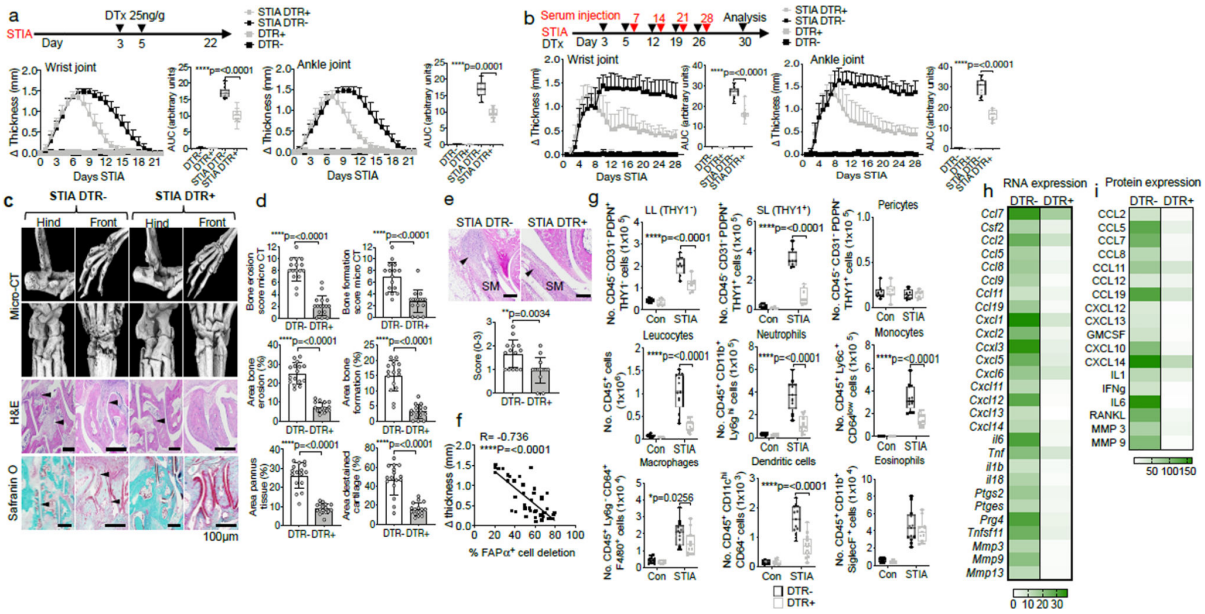

Fig. 2. Deletion of FAPα expressing cells attenuates synovial inflammation.

(**a**) Joint inflammation in deleted (STIA DTR^{+}, n=13) versus non-deleted (STIA DTR^{-}, n=9) STIA mice compared to non-arthritic deleted (DTR^{+}, n=6) and non-deleted (DTR^{-}, n=6) mice, with AUC analysis. (**b**) Effect of sustained FAPα cell deletion on joint inflammation in persistent STIA (STIA, DTR^{+}/DTR^{-} n=8 mice, and non-arthritic DTR^{+}/DTR^{-}, n=4 mice), with AUC analysis. (**c**) Representative micro-CT and histological images of day 28 persistent STIA mice with (**d**) quantification of micro-CT data, osteoclast number and histomorphometric analysis of bone erosion, pannus formation and cartilage damage, arrows indicate areas of interest (all: n=16 mice per group). (**e**) Representative histology at day 9 STIA and quantification (n=14 mice per group), arrow shows leucocyte infiltration and SM=synovial membrane. (**f**) Spearman's correlation between the percentage of FAPα cell deletion achieved at day 9 and change in ankle joint thickness (n=45 mice). (**g**) Quantification of the number of fibroblasts and pericytes (n=8 mice) and (**h**) leucocyte subsets (n=13 mice) in day 9 STIA synovia analysed by flow cytometry. (**i**) Expression of selected mRNA transcripts and proteins (by luminex analysis following stimulation *ex vivo* with TNFα) in the synovia of DTR^{-} and DTR^{+} day 9 STIA mice following DTx treatment, expressed as fold change in expression compared to non-arthritic mice (n=8 mice per group for mRNA and n=6 mice per group for protein analysis). Statistics: 1-way ANOVA with Dunnett's multiple comparison test **a**,**b**, two-tailed paired Student's t-test (**d,e**), 2-way ANOVA with Tukey's multiple comparison test (**f,g**). Data represented as Mean±S.D., except AUC analysis (in **a** and **b**) and **f,g,** which are shown as box plots (centre line, median; box limits, upper and lower quartiles; whiskers, maximum and minimum values).

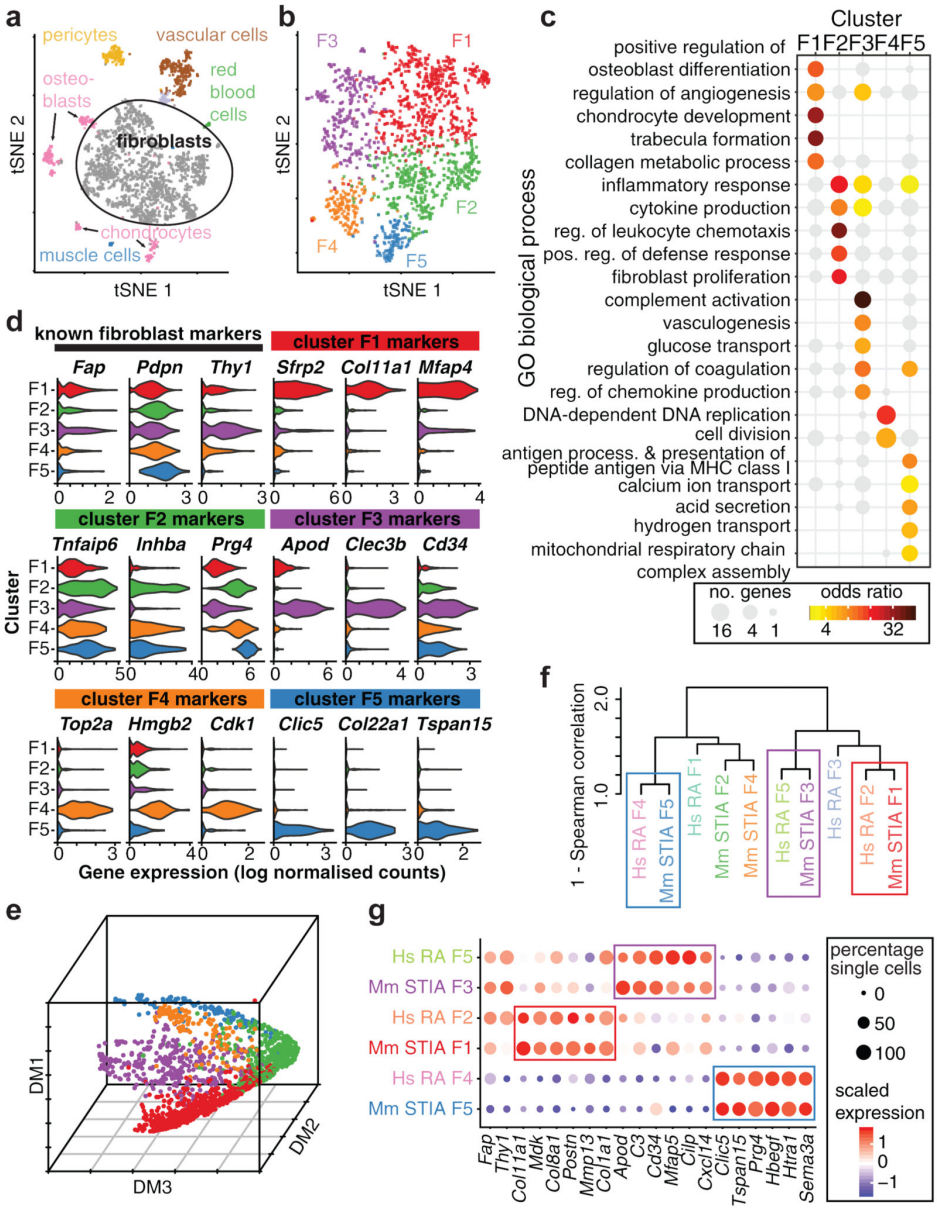

Fig. 3. Single-cell RNA-sequencing reveals distinct fibroblast subsets.

(**a**) t-SNE projection showing 2814 non-hematopoietic (CD45$^-$ CD31$^-$ cells) stromal cells from the inflamed synovium of day 9 STIA mice (n=3 biological replicates). Cells are coloured according to major cell type based on expression of known marker genes (Extended data 4 and 5). (**b**) Unsupervised graph-based clustering[16] of fibroblasts (n=1725 cells) reveals five subsets (F1-F5) in the inflamed STIA joints. For (**c**) and (**d**) conserved cluster marker genes were first identified as those with a maximum BH adjusted p value < 0.1 in separate tests of cells from each of the n=3 biological replicates (two-sided Wilcoxon

Europe PMC Funders Author Manuscripts

tests, supplementary table 1). (**c**) Over-representation analysis of Gene Ontology (GO) categories suggests different functions for the five STIA fibroblast subsets. Significant enrichments amongst cluster markers (BH adjusted $p < 0.05$, one-sided Fisher's exact tests, supplementary table 2) are shown in colour. (**d**) Expression of marker genes (x axes) in the identified STIA fibroblast clusters (y axes). The first panels show expression of known pan-fibroblast markers. The remaining sets of panels show examples of identified conserved makers genes for each fibroblast cluster F1-F5. (**e**) Embedding of the STIA fibroblasts in the first three components of a diffusion reveals possible relationships between the clusters. (**f**) Comparison of the fibroblasts clusters from the mouse (Mm) STIA model with those from human (Hs) RA patients[15]. Hierarchical clustering of orthologous (one-to-one) cluster markers identified three sets of homologous subpopulations. (**g**) Selected markers commonly expressed between homologous human and mouse clusters.

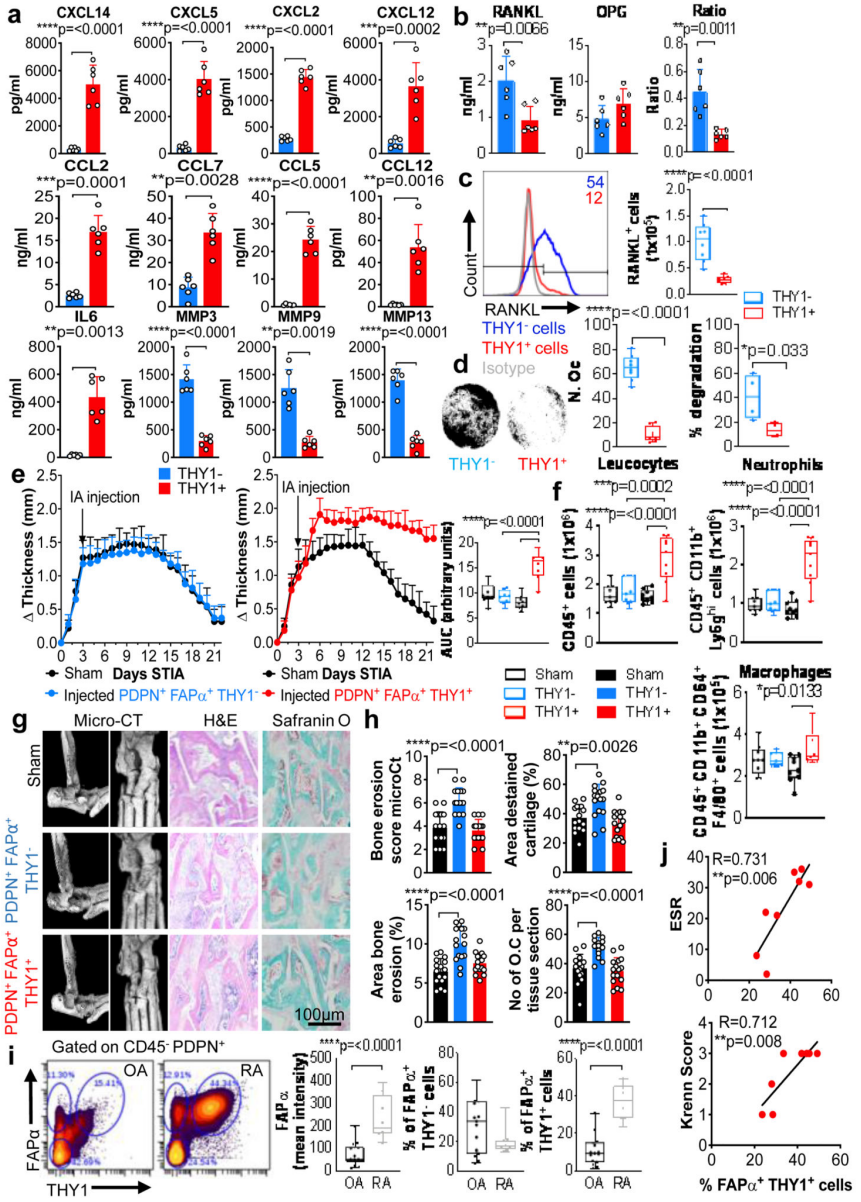

Fig. 4. Fibroblast subsets are responsible for different aspects of disease pathology.

(**a**) Luminex analysis of stimulated FAPα$^+$ THY1$^-$ and FAPα$^+$ THY1$^+$ cells isolated from day 9 STIA synovia, (**b**) secretion of RANKL and OPG (n=6 mice per group) and (**c**) quantification of the synovial RANKL$^+$ THY1$^{-/+}$ cells by flow cytometry (numbers=percentage of cells, n=8 mice per group). (**d**) Effect of FAPα$^+$ THY1$^-$ and FAPα$^+$ THY1$^+$ cells on the number of osteoclasts, N. Oc, (n=4 mice per group) and matrix degradation *in vitro* (n=8 mice per group). (**e**) Effect of IA injection of PDPN$^+$ FAPα$^+$ THY1$^-$ or PDPN$^+$ FAPα$^+$ THY1$^+$ cells into the ankle joints of day 3 STIA mice compared

Europe PMC Funders Author Manuscripts

to contra-lateral sham injected joints, with AUC analysis (n=8 mice per group). (**f**) Flow cytometric analysis of absolute number of leucocyte subsets isolated from the digested synovia of injected joints at day 12 (n=8 mice per group). (**g**) Representative images at day 12 and (**h**) quantification of micro-CT data, and histomorphometric analysis of osteoclast number, cartilage damage, bone erosion and synovial pannus (n=16 mice per group). (**i**) Mass cytometry (CyToF) analysis of $PDPN^+$ $FAP\alpha^+$ and $THY1^{+/-}$ cells in synovium of patients with OA and RA (n=15 OA, n=8 RA patient samples). (**j**) Spearman's correlation between $THY1^+$ $FAP\alpha^+$ cells in RA and serum ESR level and synovial Krenn score (n=8 RA patient samples). Statistics: two-tailed paired Student's t-test (**a-d,l**), 1-way ANOVA with Dunnett's post hoc test compared to sham injected (**e,f**), two-tailed paired Student's t-test (AUC, **e and f,h**). Data represented as Mean±S.D., except **c,d,f,l** and AUC analysis in **e,** which are shown as box plots (centre line, median; box limits, upper and lower quartiles; whiskers, maximum and minimum values).